Neuron

Article

Cooling of Medial Septum Reveals Theta Phase Lag Coordination of Hippocampal Cell Assemblies

Graphical Abstract

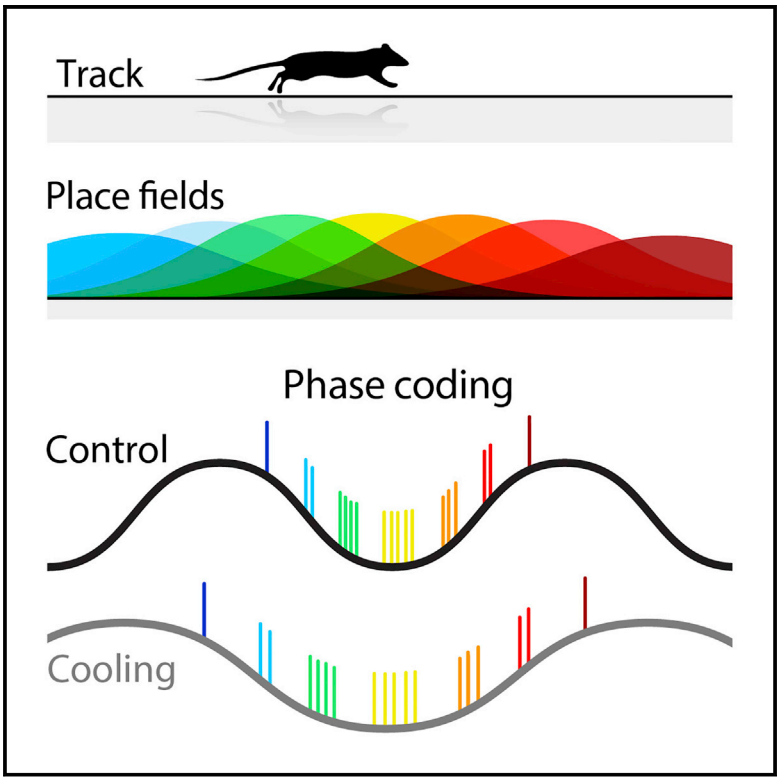

Highlights

- Cooling the medial septum slowed down theta oscillations in the hippocampus
- The spatial representation in the hippocampus remained intact
- Choice errors increased in a spatial task
- Distance-time, but not distance-theta phase, compression was altered

Authors

Peter Christian Petersen,
György Buzsáki

Correspondence

gyorgy.buzsaki@nyulangone.org

In Brief

Petersen et al. demonstrate that cooling of the medial septum slows theta oscillation and increases choice errors without affecting spatial features of pyramidal neurons. Cooling affects distance-time, but not distance-theta phase, compression. The findings reveal that cell assemblies are organized by theta phase and not by external (clock) time.

Petersen & Buzsáki, 2020, Neuron *107*, 1–14
August 19, 2020
https://doi.org/10.1016/j.neuron.2020.05.023

CellPress

Neuron

CellPress

Article

Cooling of Medial Septum Reveals Theta Phase Lag Coordination of Hippocampal Cell Assemblies

Peter Christian Petersen[1] and György Buzsáki[1,2,3,4,*]
[1]Neuroscience Institute, NYU Langone, New York University, New York, NY 10016, USA
[2]Department of Neurology, NYU Langone, New York University, New York, NY 10016, USA
[3]Center for Neural Science, New York University, New York, NY 10003, USA
[4]Lead Contact
*Correspondence: gyorgy.buzsaki@nyulangone.org
https://doi.org/10.1016/j.neuron.2020.05.023

SUMMARY

Hippocampal theta oscillations coordinate neuronal firing to support memory and spatial navigation. The medial septum (MS) is critical in theta generation by two possible mechanisms: either a unitary "pacemaker" timing signal is imposed on the hippocampal system, or it may assist in organizing target subcircuits within the phase space of theta oscillations. We used temperature manipulation of the MS to test these models. Cooling of the MS reduced both theta frequency and power and was associated with an enhanced incidence of errors in a spatial navigation task, but it did not affect spatial correlates of neurons. MS cooling decreased theta frequency oscillations of place cells and reduced distance-time compression but preserved distance-phase compression of place field sequences within the theta cycle. Thus, the septum is critical for sustaining precise theta phase coordination of cell assemblies in the hippocampal system, a mechanism needed for spatial memory.

INTRODUCTION

Theta frequency oscillations coordinate neuronal activity in the hippocampus-subicular-entorhinal complex and entrain neurons in various neocortical areas (Buzsáki, 2002). Damage or inactivation of the medial septum (MS)/diagonal band abolishes theta oscillations in all these areas (Petsche et al., 1962; Vertes and Kocsis, 1997) and is associated with impairment of memory, spatial navigation, and other cognitive functions (Bolding et al., 2020; Brandon et al., 2011; Chang and Gold, 2004; Chrobak et al., 1989; Givens and Olton, 1990; Jeffery et al., 1995; Leutgeb and Mizumori, 1999; Wang et al., 2015; Winson, 1978). However, whether the behavioral impairment is due to silencing or damaging important septal afferents or to the absence of theta-phase-multiplexed coordination of activity of neurons (Harris et al., 2003; Kay et al., 2020) in the hippocampal system has remained an unsolved challenge. Such dissociation is not straightforward, because manipulations that abolish theta also affect neurons and synapses, which may exert their own, theta-independent effects.

Early experiments suggested that the MS acts as a "pacemaker," sending out synchronous outputs, akin to a conductor of an orchestra (Borhegyi et al., 2004; Petsche et al., 1962; Stewart and Fox, 1990; Sweeney et al., 1992; Zutshi et al., 2018), followed by models in which cholinergic and GABAergic neurons of MS fire at distinct unique phases of the theta cycle (Borhegyi et al., 2004; Petsche et al., 1962; Stewart and Fox, 1990; Sweeney et al., 1992). Yet, rather than being a simple rhythm generator, several recent works imply a more intricate involvement of the MS in coordinating activity patterns in the hippocampal-entorhinal system. First, hippocampal neurons are not locked synchronously to a spatially coherent rhythm but show a systematic phase shift up to 270° in the CA1-CA3-dentate gyrus axis and different layers of the entorhinal cortex (Buzsáki et al., 1986; Mizuseki et al., 2009). Second, theta is not synchronous over the entire septotemporal axis but instead shifts gradually as much as 180° from the septal to the temporal pole (Lubenov and Siapas, 2009; Patel et al., 2012). Third, all activated principal cells, such as neurons that fire at particular spatial positions (place cells; O'Keefe and Nadel, 1978; O'Keefe and Recce, 1993) or in a given memory episode (Pastalkova et al., 2008), oscillate faster than the local field potential (LFP) theta. The oscillation frequency of place cells correlates inversely with the diverse sizes of place fields (Dragoi and Buzsáki, 2006) and varies systematically along the septotemporal axis (Kjelstrup et al., 2008; Maurer et al., 2006; Royer et al., 2010). Similarly, theta oscillation frequency of grid cells in the entorhinal cortex decreases progressively in the dorsoventral direction (Giocomo et al., 2007), providing a frequency match between corresponding entorhinal and hippocampal neurons. Finally, a phase interference has been described between single neurons and population theta-rhythmicity (Skaggs et al., 1996; Geisler et al., 2010), as shown by a progressive backward phase shift of pyramidal cells' spikes (phase precession; O'Keefe and Recce, 1993). In summary, spikes of principal cells in the limbic system occur at all phases of the theta cycle, and all active principal cells oscillate

Please cite this article in press as: Petersen and Buzsáki, Cooling of Medial Septum Reveals Theta Phase Lag Coordination of Hippocampal Cell Assemblies, Neuron (2020), https://doi.org/10.1016/j.neuron.2020.05.023

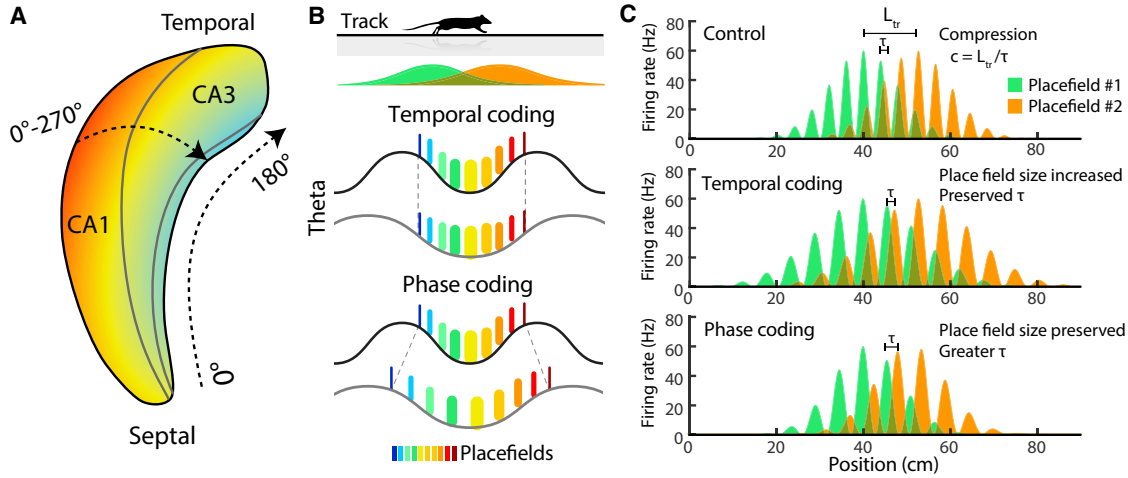

Figure 1. Theta Phase Dynamics and Connectivity in the MS-Hippocampal System

(A) Theta oscillation is a traveling wave and shows systematic phase shift in both the septo-temporal and CA1-CA3-dentate gyrus axes (color scale illustrates the phase offsets between regions). Hippocampal neurons are not locked synchronously to a global theta rhythm but show a systematic phase shift up to 270° in the CA1-CA3-dentate gyrus axis and a gradual 180° shift from the septal to the temporal pole (Lubenov and Siapas, 2009; Patel et al., 2012).

(B) Hypothetical effects of MS cooling on within-theta neuronal assembly organization. Top: two spatially overlapping place fields along the track. Middle: time lags between place cell assemblies (different color ticks) remain unchanged with theta cycle lengthening (gray). Bottom: place cells assemblies expand in time but keep their theta phase relationships.

(C) Theta cycle relationship between overlapping place fields of the same size (L_{PF}) of two place cells (green and tangerine). The travel distance (L_{tr}) between the peaks of the two place fields is correlated with the time offset (τ) of spikes between the place neurons (Dragoi and Buzsáki, 2006). The ratio of travel distance and theta timescale time lag defines distance to time compression ($c = L_{tr} / \tau$; Geisler et al., 2010). Middle and bottom: hypothetical effects of MS cooling. Middle: place field size changes but τ is preserved. Bottom: fewer theta cycles occur within the same size place field and τ increases.

faster than the global LFP theta, whose instantaneous frequency co-varies coherently across subregions and structures (Figure 1). These experiments suggest a more elaborate involvement of MS circuit in theta-cycle phasing of hippocampal neuronal assemblies than the current models would imply (Borhegyi et al., 2004; Buzsáki, 2002; Hangya et al., 2009; Stewart and Fox, 1990).

Damaging, silencing, or pharmacological perturbation of the MS circuit (Bolding et al., 2020) cannot effectively address temporal/theta phase coordination issues. Perturbation studies using synchronizing electrical (McNaughton et al., 2006) or optogenetic (Dannenberg et al., 2019; Vandecasteele et al., 2014; Zutshi et al., 2018) stimulation may not be effective either to fully examine this problem because strong pulses impose global synchrony on all neurons unlike the time-shifted patterns observed under physiological conditions (Lubenov and Siapas, 2009; Patel et al., 2012). Therefore, we used temperature manipulation, an approach that is applicable to localizing the origin of temporal coordination (Fee and Long, 2011). In contrast to unwanted synchronizing stimulation, cooling does not damage neurons or interrupt local interactions but alters multiple parameters of neurons from channel kinetics to transmitter release, resulting in temporal warping of circuit dynamic (Katz et al., 2004; Thompson et al., 1985; Volgushev et al., 2000). For example, reducing temperature in the vocal center of the zebra finch elongated the bird's song by proportionally slowing its acoustic microstructure (Long and Fee, 2008).

By cooling the MS, we examined how slowing theta oscillations affect hippocampal network activity, physiological properties of neurons, and their spatial correlates (O'Keefe and Nadel, 1978). Several models assume that the phase interference between MS theta oscillation (LFP theta) and the faster spike periodicity of place cells and grid cells, driven by a hypothetical "spatial input," determines the slope of spike phase precession and, consequently, place field size (Burgess et al., 2007; Chadwick et al., 2016; Harvey et al., 2009; Kamondi et al., 1998; O'Keefe and Recce, 1993; Zutshi et al., 2018). A prediction of these models, therefore, is that slowing MS-driven theta oscillation should affect the size of place fields by increasing the difference between the frequencies of the two oscillators. Each theta cycle contains a sequence of place cell assemblies that corresponds to the sequences of upcoming place cells on the maze (Dragoi and Buzsáki, 2006; Maurer et al., 2012). If the temporal lags within cell assemblies are preserved, more assemblies can be packaged in a wider theta cycle (temporal coding). An alternative hypothesis is that the fundamental organization in the septo-hippocampal system is not time but phase based (phase coding). Under the phase model, theta phase assembly coordination should remain unaltered but at the expense of affecting timing between place cell assemblies (Figure 1). Our results favor the phase coding model of theta cycle coordination.

RESULTS

MS Cooling Decreases Hippocampal Theta Frequency and Power

To achieve localized cooling of the MS, we constructed a cryoprobe, consisting of a silver wire (125 μm in diameter), 25-μm

Please cite this article in press as: Petersen and Buzsáki, Cooling of Medial Septum Reveals Theta Phase Lag Coordination of Hippocampal Cell Assemblies, Neuron (2020), https://doi.org/10.1016/j.neuron.2020.05.023

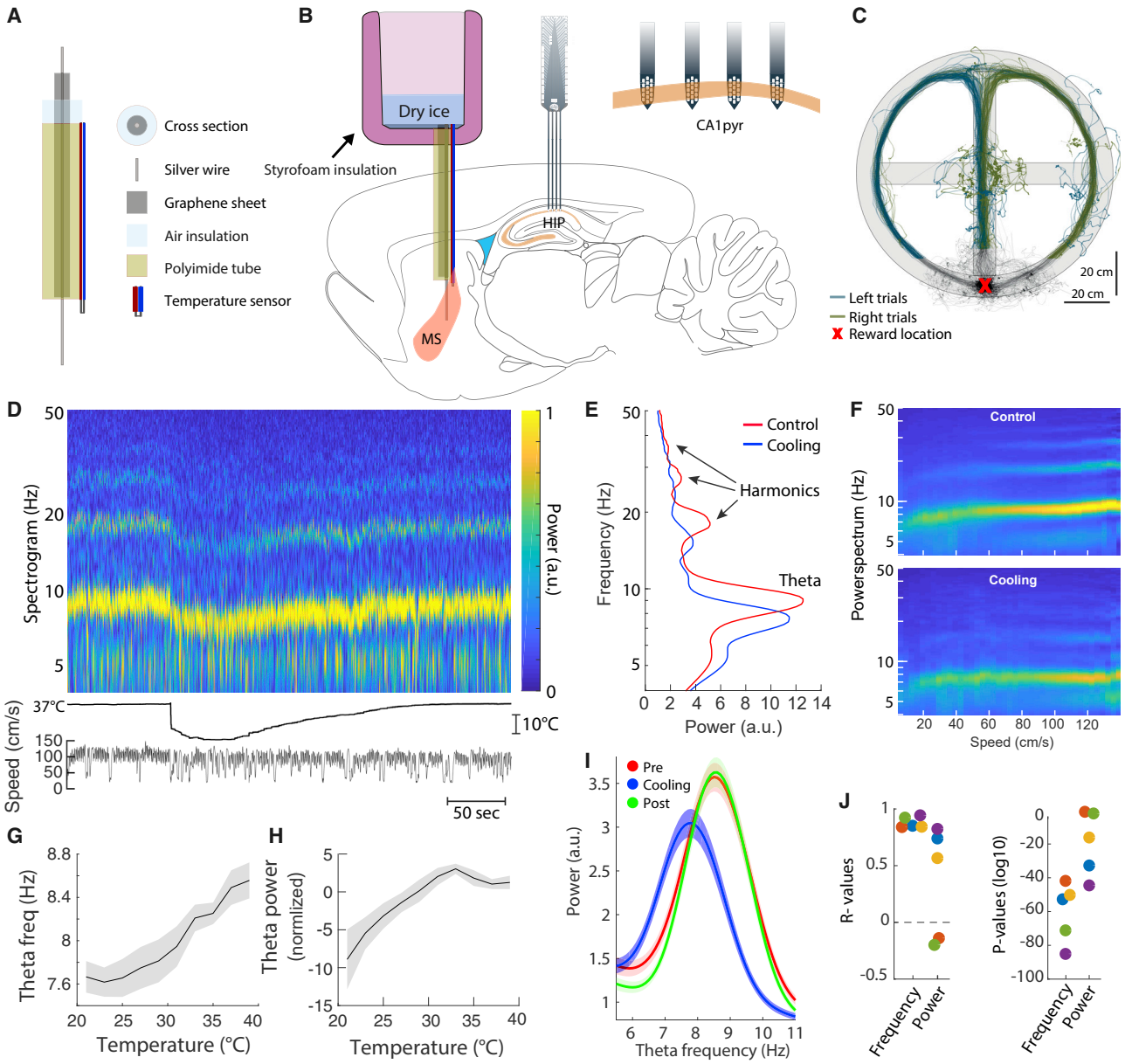

Figure 2. Cooling of MS Affects Theta Oscillations

(A) Components of the cooling probe.

(B) Cooling probe and thermocouple are implanted in MS and silicon probes in the hippocampus. Dry ice is placed into the reservoir and MS is cooled by thermal conduction.

(C) Maze with left (blue) and right (green) run trajectories superimposed.

(D) Top: time-resolved spectrogram in a single session. Color scale is normalized. Middle: temperature. Bottom: running speed of the animal.

(E) Frequency spectrum with power of theta and its first to third harmonics (arrows).

(F) Power spectra of the theta band and harmonics before (top) and after (bottom) cooling. Color scale is normalized. Same single session used in (D)–(F).

(G and H) Effect of MS cooling on theta frequency (G) and power (H) showing group data for all sessions and subjects (mean values with SE).

(I) Group data for theta frequency and power before, during, and after MS cooling.

(J) R and p values for theta frequency and power in individual rats (color coded).

Data are from 53 sessions in five rats (G–J).

graphene sheet, air isolation, and a polyimide tube (Figure 2A; see STAR Methods). The back end of the silver wire was coiled at the bottom of an insulated reservoir. Cooling was achieved by filling the reservoir with dry ice (−78.5°C). The protruding tip (1.5 mm) of the front-end wire was implanted into the MS diagonal band area (Figure 2B). A temperature sensor (k-type

Please cite this article in press as: Petersen and Buzsáki, Cooling of Medial Septum Reveals Theta Phase Lag Coordination of Hippocampal Cell Assemblies, Neuron (2020), https://doi.org/10.1016/j.neuron.2020.05.023

thermocouple; two 80-μm wires) was attached to the outer surface of the cryoprobe cannula to continuously monitor local temperature (Figure 2A; Figure S1). Pilot experiments were performed to perfect the device so that hippocampal theta frequency could be reduced for 5–15 min (Figure S1).

In addition to the cooling probe, five rats were also implanted with multi-shank 64-site silicon probes bilaterally in the CA1 pyramidal layer of the dorsal hippocampus (STAR Methods) and trained in a figure-8 maze (spontaneous alternation task; Figure 2B) to run for water reward. After a block of control trials (~40 trials), dry ice was placed into the reservoir, which reduced MS temperature for ~15 min (or corresponding to ~20–60 "cooling" trials), followed by recovery trials (20–80). MS cooling induced fast and reversible change in the frequency and power of hippocampal theta oscillations (Figures 2D–2F and 2I). Theta frequency decreased linearly with MS temperature (Figure 2G; down to 20°C; R = 0.81; $p = 5.4 \times 10^{-48}$), and this relationship was more consistent across animals than the effect on theta power ($R = 0.54$; $p = 1.2 \times 10^{-16}$; Figures 2G and 2H). The time course of theta-frequency decrease, and less so its power, mirrored the temporal dynamic of MS cooling (see time course in Figure 6).

In a control experiment, we measured temperature simultaneously in the MS and hippocampus, and found a <1.5°C decrease in the hippocampus at the time of the largest MS temperature decrease (16°C), which is within the physiological range of brain temperature (Figures S1H–S1K; Moser and Andersen, 1994). Critically, in contrast to the rapid onset of MS cooling (maximum effect at ~45 s; time constant: 11 s), the mild temperature decrease in the hippocampus was considerably delayed (peak at 115 s; time constant 48 s for the right hippocampus, and 72 s for the left). Furthermore, firing rates of both pyramidal cells and putative interneurons in the hippocampus decreased immediately after MS cooling, and the changes correlated with MS temperature change (see Figures S5G and S5H) rather than with the delayed minimal temperature decrease in the hippocampus. Finally, the waveforms of action potentials in the hippocampus, a sensitive measure of temperature change (Thompson et al., 1985; Volgushev et al., 2000), were not affected by MS cooling (Figure S1G). Overall, these findings show that MS cooling had an immediate and strong effect on LFP theta and suggest that these changes were not a consequence of the spread of cooling to the hippocampus.

Effect of MS Cooling on Place Field Features

Spatial parameters of place fields were largely left unaffected by MS cooling. Place field size (L_{PF}) remained highly correlated before and after MS cooling (Figures 3A–3C; see Figure S3 for other place field features). L_{PF} and f_p were negatively correlated (Dragoi and Buzsáki, 2006; O'Keefe and Recce, 1993), and this relationship was not altered by cooling, as illustrated by the similar slopes, even though the intercept of the regression line during cooling slightly decreased (Figures 3C and 3D).

Next, we compared measured place field size with model-based calculations. Previous studies have demonstrated a quantitative relationship among theta frequency (f_{LFP}), oscillation frequency of pyramidal cells within their place fields (f_p), the duration it takes the rat to run across the place field (D_{PF}), place field size (S_{PF}), and the rat's velocity (v) (Geisler et al., 2010). Since $D_{PF} = 1/(f_p - f_{LFP})$ (Geisler et al., 2010) and D_{PF} can be calculated by dividing place field size (S_{PF}) with locomotion velocity within the place field ($S_{PF} = D_{PF}{}^{*}v$), place field size can be derived from $S_{PF} = v/(f_p - f_{LFP})$. We found a reliable and similar relationships between measured place field sizes and model-predicted sizes for trials before (R = 0.55), during (R = 0.54), and after (R = 0.11) MS cooling (Figure 3E). Information content of place cell spikes was also left unaltered by MS cooling ($p > 0.26$; Figure 3F).

We also investigated potential changes to the scale of distance representation at the population level resulting from MS cooling. We calculated the correlations between pairs of population vectors of unit firing constructed from binned rate maps (Gothard et al., 1996). The distance in maze corridor bins at which the spatial population vector correlation function dropped to 0.5 was used as a measure of the scale of the spatial representation, a measure independent of arbitrary definition of place field (Gothard et al., 1996). Population vector correlation of pyramidal cells was not affected by MS cooling (Figures 3G and 3H). This analysis further suggested that spatial representation by place cell population was largely unaffected by MS cooling (Figure 3I).

Effects of MS Cooling on Single-Neuron Properties

In contrast to the lack of changes of spatial features, MS cooling induced widespread but correlated physiological effects (Figure 4). The theta oscillation frequency of pyramidal neurons decreased linearly and paralleled the downward frequency shift of LFP theta oscillation (Figure 4A; f_{LFP}: R = 0.66, slope = 0.071. f_p: R = 0.38, slope = 0.09). Theta frequency oscillation of putative fast spiking interneurons also decelerated (Figure S2D), commensurate with the downward frequency shift of LFP theta oscillation.

The range of within-field oscillation frequency of place cells (f_p) was larger compared to the range of LFP theta frequency within place fields both before and during MS cooling (f_{LFP}; Figure 4C), corresponding to the range of place field sizes. MS cooling decreased both f_p and f_{LFP}, measured within the place fields of neurons, by approximately the same degree (Figure 4B and 4C; $f_{LFP\ pre} = 8.4 \pm 0.38$, $f_{LFP\ cooling} = 7.7 \pm 0.36$, $f_{LFP\ post} = 8.5 \pm 0.29$; $f_{p\ pre} = 10.6 \pm 0.95$, $f_{p\ cooling} = 9.5 \pm 0.84$, $f_{p\ post} = 10.4 \pm 0.72$, n = 365). Both values recovered after cooling. The y intercepts of regression lines of the f_p versus f_{LFP} relationship shifted from pre-cooling to cooling but remained parallel to each other in each condition. The lines connecting the centers of masses also remained largely parallel with the diagonal (Figure 4C), indicating preserved $f_p - f_{LFP}$ differences. Both within-field and peak firing rates of place cells decreased moderately during MS cooling (Figure S2; 11% and 12%; $p < 10^{-9}$ and $p < 10^{-11}$, respectively; see time course in Figure S5). Interneuron firing rates also decreased by approximately the same degree (Figure S2). The slope of the relationship between travel distance across the place field and phase advancement of spikes (phase precession index; O'Keefe and Recce, 1993) decreased slightly, but nevertheless significantly, during MS cooling (Figure 4D).

Since previous studies showed that the running speed of the animal is correlated with several physiological parameters

Please cite this article in press as: Petersen and Buzsáki, Cooling of Medial Septum Reveals Theta Phase Lag Coordination of Hippocampal Cell Assemblies, Neuron (2020), https://doi.org/10.1016/j.neuron.2020.05.023

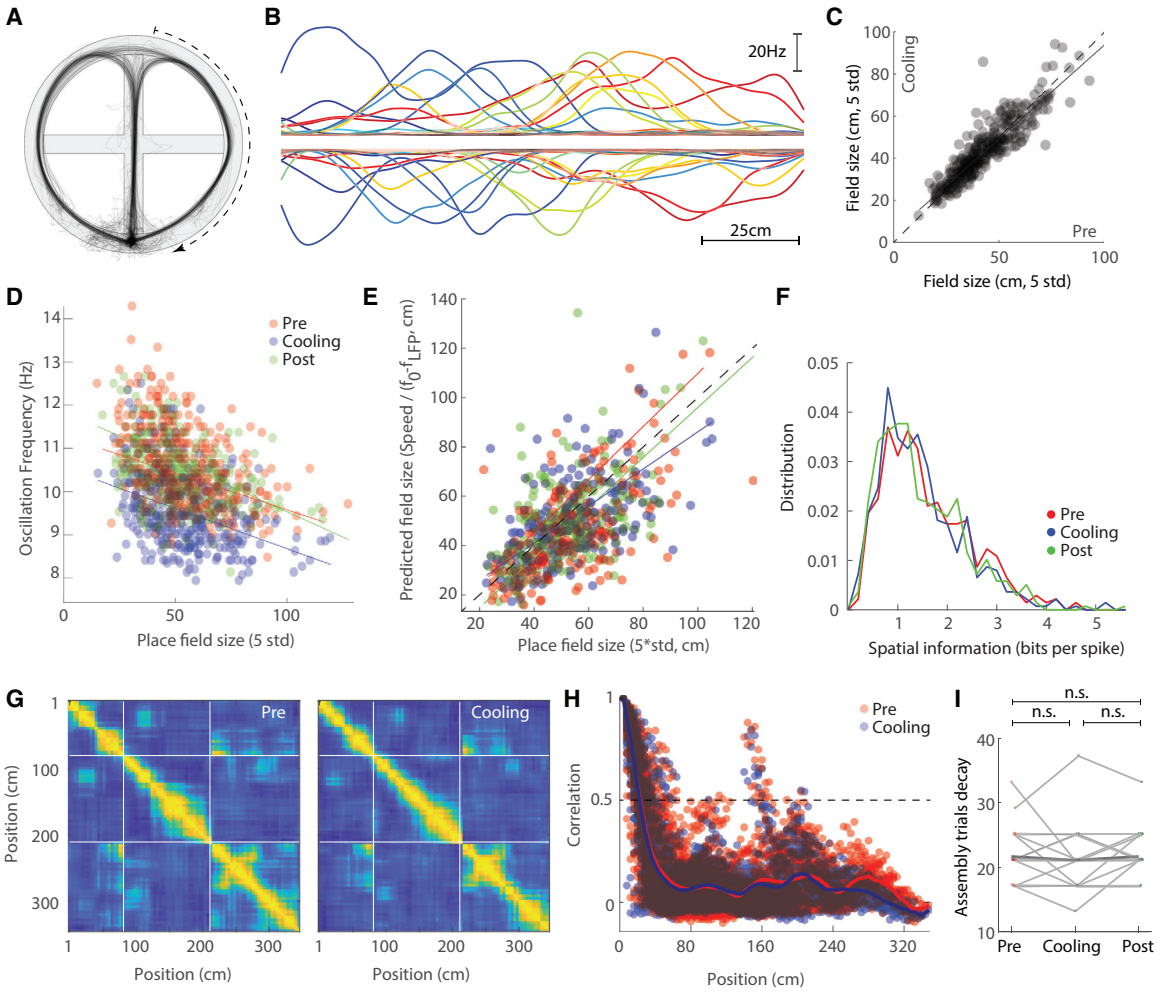

Figure 3. Place Field Features Are Not Affected by MS Cooling

(A) Example of right arm runs in the T maze.

(B) Place fields in the right arm before (upward traces) and during MS cooling (downward traces) in a single session. Note the preserved size, position, and shape of place fields.

(C) Place field size does not change with MS cooling (R = 0.91).

(D) Place field size continues to be inversely correlated with f_p after MS cooling ($R_{pre} = -0.49$; $R_{cooling} = -0.40$; $R_{post} = -0.40$. $p < 10^{-9}$ all conditions).

(E) Correlation between measured (x) and model-predicted (y) size of place fields before, during, and after MS cooling. Place field size in the model (Geisler et al., 2010) was derived from $S_{PF} = v/(f_p - f_{LFP})$. v = speed.

(F) Information content of place cell spikes. None of the comparisons are significantly different ($p > 0.26$).

(G) Population vector cross-correlation matrices from a single session from baseline (pre-cooling) and MS cooling trials. The higher (yellow) values indicate that the correlation of population activity is relatively constant between neighboring positions. White lines mark the boundaries between the central, right, and left arms. Normalized color scales are the same in the two panels.

(H) Population vector change as a function of distance. Superimposed decorrelation curves (cross-diagonal values in (G) for trials before (red) and during MS cooling (blue). To quantify the scale of the spatial representation, the interval at which the correlation dropped to 0.5 was calculated for each session (dashed line).

(I) Decorrelation values for data from 21 sessions.

(Dannenberg et al., 2019; Diba and Buzsáki, 2008; Fuhrmann et al., 2015; Geisler et al., 2007; Maurer et al., 2012; McNaughton et al., 1983), we aimed to disambiguate the effect of MS cooling and running speed. Running speed decreased relatively monotonically within session (Figure 4E; see also Figure 5C). The animal's speed correlated with both theta power and f_p (Figures 4F and 4G). Yet, f_p changes during MS cooling could not be explained by decreased running velocity of the rat, because f_p values during cooling were lower at all velocities (Figure 4G).

We examined the relationship between running speed and LFP theta frequency (f_{LFP}) in two different ways. The first comparison was done on a trial basis, comparing the mean theta frequency with the mean running speed in each trial. This comparison showed a positive correlation before, during, and after MS cooling, with the largest changes taking place at lower running speeds (10 to 40 cm/s; Figure S2E). However, this comparison cannot dissociate the effect of speed from the effect of maze environment (Montgomery et al., 2009). Therefore, we quantified

Please cite this article in press as: Petersen and Buzsáki, Cooling of Medial Septum Reveals Theta Phase Lag Coordination of Hippocampal Cell Assemblies, Neuron (2020), https://doi.org/10.1016/j.neuron.2020.05.023

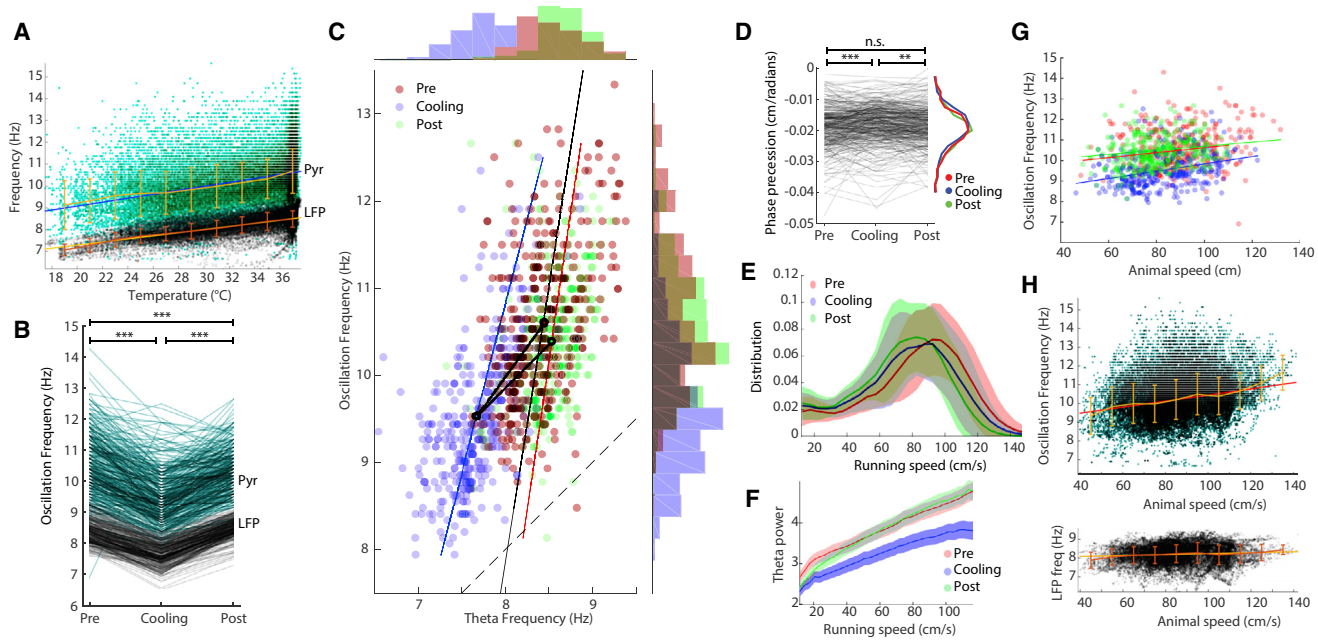

Figure 4. Effects of MS Cooling on Single-Unit Parameters

(A) LFP theta frequency (f_{LFP}) and oscillation frequency of place cells (f_p) as a function of MS temperature. Each dot is a trial average measured within a single place field. Note parallel changes between f_p (green) and f_{LFP} (black).

(B) Oscillation frequency shown separately for all place cells (f_p; gray) and LFP theta frequency (f_{LFP}; black) measured in the corresponding place fields before, during, and after MS cooling. ***p < 5.9e−8.

(C) Correlation between LFP theta frequency (f_{LFP}) and place cell oscillation frequency (f_p; $R_{pre} = 0.61$; $R_{cooling} = 0.59$; $R_{post} = 0.36$; $p < 10^{-19}$ each). Black lines connect the centers of mass of each cloud. Marginal histograms show the distribution of f_p of place cells and f_{LFP} in the corresponding place fields. Dashed line: diagonal.

(D) Theta phase precession slopes of place cell spikes before, during, and after MS cooling. **p < 0.007; ***p < 0.0003.

(E) Distribution of running speeds in all sessions (n = 53).

(F) Theta power as a function of running speed.

(G) Place cell oscillation frequency (f_p) as a function of running speed, measured in each place field.

(H) f_p and f_{LFP} as a function of running speed. As in (G), but trials before, during, and after MS cooling are pooled to show that f_p depends more strongly on running speed than f_{LFP}.

the speed/theta frequency relationship within each place field (f_{LFP}), together with the oscillation frequency of the corresponding place cell (f_p). This calculation revealed that while speed exerted a relatively linear effect on f_p, it had no or little effect on the frequency of f_{LFP} (Figure 4H; Czurkó et al., 1999; Montgomery et al., 2009) within the dominant speed range of the rat. As a result, the $f_p - f_{LFP}$ difference increased with running velocity. This is in contrast to the effect of MS cooling, after which the difference between f_p and f_{LFP} was preserved (Figures 4A and 4C). Finally, we examined duration of theta cycles as function of the rat's position on the track. While theta duration was consistently longer during MS cooling trials, duration distribution did not correlate with the speed distribution on the track (Figure S3). Overall, these findings indicate that the physiological effects of MS cooling are dissociable from running speed effects (Tsanov, 2017).

MS Temperature Effects on Theta Time/Phase Compression of Place Cell Sequences

Our findings so far revealed a contrast between consistent changes in physiological parameters of single neurons and the stability of their place field features by MS cooling. Because single-neuron features do not inform us about their theta-organized assembly properties, we next examined the temporal sequences of place cell assemblies in the theta cycle (Figures 5A and 5B). The distances between place cell peaks (L_{tr}) are known to correlate with their theta-scale time lags (τ) and phase lags, and the ratio of L_{tr} and τ is known as distance-time compression (c; Figure 1A; Dragoi and Buzsáki, 2006; O'Keefe and Recce, 1993). To display the dynamics of ensemble compression of place cell distances as the animal passes through sequential positions on the maze, we plotted the sequence compression for the entire population of place cell pairs over several theta cycles within a 0.8-s period. In Figure 5C, each dot corresponds to the time difference of spike occurrences of place neuron pairs (τ), averaged across all trials of a session (n = 18 sessions in five rats). This representation mimics the spatial-temporal evolution of spiking of all pyramidal neurons in the dorsal hippocampus as the rat traverses the place field center of a reference neuron (Dragoi and Buzsáki, 2006). The "clouds" are spaced by theta-scale intervals, relating to the joined oscillating frequency of place cell pairs, and the slope of the clouds corresponds to the distance-to-theta

Please cite this article in press as: Petersen and Buzsáki, Cooling of Medial Septum Reveals Theta Phase Lag Coordination of Hippocampal Cell Assemblies, Neuron (2020), https://doi.org/10.1016/j.neuron.2020.05.023

CellPress

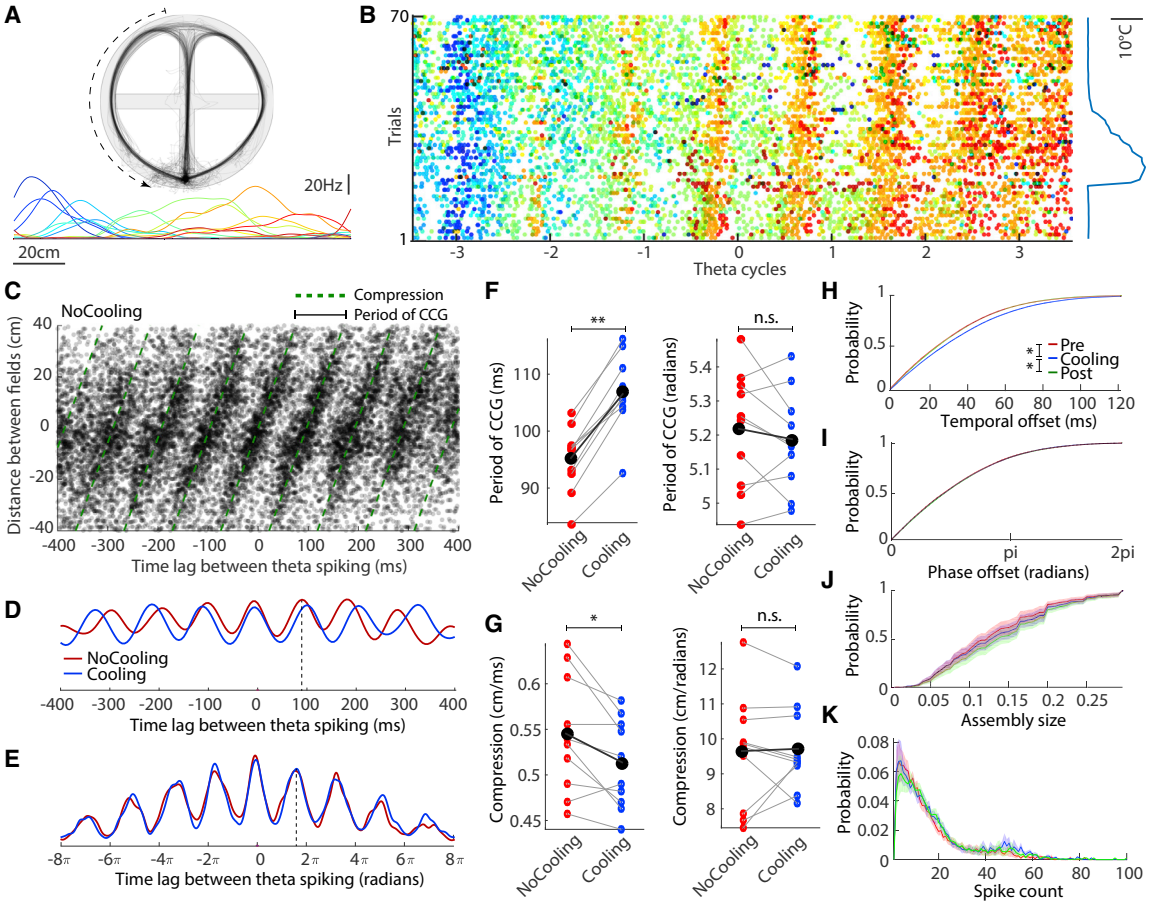

Figure 5. Distance-Theta Timescale Compression Is Affected by MS Cooling

(A) Selected place fields in the left arm of the maze before MS cooling in a single session.

(B) Within-theta cell assemblies. Each row of dots is a trial of the spiking activity of place cells (same color code as in (A) in successive theta cycles). 0 is the theta cycle in the middle of the left arm. Note shifting cell assemblies in successive theta cycles (from blue to red) and preserved phase preference of place cell spikes during and after MS cooling (right trace).

(C) Relationship between distances of place field peaks across neuron pairs (y axis) and their theta time-scale cross-correlogram lags (τ on x axis; as in Figure 1C) during trials prior to MS cooling (2,948 = pairs across 18 sessions, five rats). Green dashed line; compression index (slope), c = 0.54 cm/ms. Period of the cross correlogram (CCG) is highlighted (black solid line).

(D) Sum of the theta repeated spike cross-correlograms of place field pairs. The red line is the sum of all dots in (C) (NoCooling); the blue line is the sum of all dots of a similar graph during cooling. Vertical dashed line indicates that the oscillation frequency of the spike cross-correlation before cooling (~85 ms) is faster that f_{LFP} (~110 ms at 9 Hz).

(E) Similar to (D), but instead of time lags, within-theta phase lags between spikes were calculated. Vertical dashed line indicates that the oscillation frequency of the spike cross-correlation is faster than that of f_{LFP} (2π).

(F) Duration of the theta-repeated spike cross-correlograms (as in D), calculated for each session, significantly increased during MS cooling, compared to control (pre- and post-cooling epochs combined) trials (**p = 0.002; two-sided signed rank test), whereas the spike phase-lag correlations remained unaffected (n.s., p = 0.32). Black disks and connected line represent group means.

(G) The compression index, c (cm/ms; i.e., the slope in C), significantly decreased during MS cooling (*p = 0.02), but the distance/phase lag compression (cm/radian) remained unaffected (p = 0.92).

(H) Cumulative distributions of theta scale time lags (τ) between place cell pairs before (pre), during, and after (post) MS cooling. MS cooling data are significantly different from both pre- and post-cooling trials (pre versus cooling p = 8.0^{-5}; post versus cooling p = 0.00032; N = 10 sessions, four rats). Pre- and post-cooling curves are strongly superimposed (pre versus post, p = 0.79).

(I) Same as in (H), but for phase lags (all comparisons are non-significant, p > 0.24).

(J) Cumulative plots of the fraction of all simultaneously recorded neurons active in the theta cycle (pre versus cooling, p = 0.28; post versus cooling, p = 0.006; pre versus post, p = 0.0005).

(K) Distribution of spike counts within theta cycles (pre- and post-cooling epochs are not different from MS cooling epochs or from each other; p > 0.058). y axis, probability.

Please cite this article in press as: Petersen and Buzsáki, Cooling of Medial Septum Reveals Theta Phase Lag Coordination of Hippocampal Cell Assemblies, Neuron (2020), https://doi.org/10.1016/j.neuron.2020.05.023

scale-time compression (*c*; Maurer et al., 2012). Several place cells are active together in each theta cycle, but the group composition varies from cycle to cycle (Figure 5B; Dragoi and Buzsáki, 2006; Maurer et al., 2012)

Both the joined oscillating frequency of place cell pairs and *c* were affected by MS cooling (Figures 5D, 5F, and 5G). Because the compression index also depends on running speed (Maurer et al., 2012), and because running speed gradually decreased across the entire session (Figures 3E and 6C), we combined trials before and after cooling into a single control group (mean running speed = 87.3 ± 8.0). During MS cooling (mean running speed = 86.2 ± 9.9), $1/f_p$ increased (i.e., f_p decreased) in each examined session relative to control runs (Figures 5F and 5G; 0.002; Wilcoxon signed rank test), whereas distance-time compression decreased (Figure 5G; $p = 0.02$). We also constructed analogous plots displaying L_{tr} versus theta phase lags of spike pairs instead of time lags. Phase lags remained unchanged after MS cooling (Figure 5F; $p > 0.24$ for all pairs; Wilcoxon signed rank test), and, as a consequence, the ratio (i.e., L_{tr} versus theta "phase compression") between L_{tr} and phase lag did not change either ($p < 0.92$; Figure 5g).

Because distances between place field peaks (L_{tr}) were not affected by MS cooling (Figures 3c and g-i) but distance-time compression decreased (Figure 5g), time lags (τ) are expected to increase. To examine this effect directly, we plotted the distributions of both theta time lags (τ) and phase lags between all pairs of place cells in each session. During MS cooling, the time lags increased significantly (Figure 5H; $p < 10^{-4}$; sign rank test; $n = 10$ sessions), whereas they were not different from each other during precooling and post-cooling sessions ($p = 0.79$), despite slower running speed during post- compared to pre-cooling trials. In contrast, phase lags between spikes of place cell pairs were not affected by MS cooling (Figure 5I; $p > 0.24$ between all conditions). Thus, theta phase lags remained similar while time lags increased.

These findings suggested that the same number of place cell assemblies were compressed into theta cycles both before after MS cooling and the assemblies were proportionally dispersed within the lengthened cycle during cooling trials (Figures 5C and 5D). In support of this hypothesis, we found that the fraction of place cells active in a given theta cycle was not significantly affected by MS cooling (Figure 5J; $p = 0.2$). The number of spikes emitted by all neurons per theta cycle was also preserved after MS cooling (Figure 5K), which might be explained by the similar magnitude of the within-field firing rate decrease of place cells (~12%; Figure S2) and theta frequency decrease (~12%; Figures 4A and 4B; for trial-wise correlations, see Figure S5).

MS Cooling Increases Behavioral Errors

The temperature decrease in the MS was immediately accompanied by increased choice errors in the maze (Figures 6A–6C). The worst memory performance occurred between trials 4 and 8 after MS cooling, when the MS temperature reached its minimum, accompanied by the largest decreases of theta frequency and power (Figure 6C; see also Figure S5). Overall, the number of memory errors increased ~3-fold, assessed either within rats ($p < 0.05$ for all animals) or across all animals ($p = 10^{-6}$; Figures 6D and 6E). The incidence of errors negatively and significantly correlated with temperature change ($R = -0.35$; $p < 0.01$; all animals) and theta frequency ($R = -0.35$; $p < 0.01$; all animals) and less so with theta power (only two of five animals had significant $R > -0.3$; $p < 0.01$), but not with the running speed of the rat (R ~0.1; $p > 0.05$ for all animals; Figures 6F–6J; see relationship to firing rates and number of spikes per theta cycle in Figure S5).

DISCUSSION

Cooling the MS reduced both LFP theta frequency and power in the hippocampus. It also resulted in more choice errors in a spatial navigation task without affecting spatial attributes of individual place cells and the spatial map. The slowing of LFP theta oscillation was paralleled with a proportionate (1) decrease of theta frequency oscillation of place cells, (2) theta time cross-correlations of place cell pairs, (3) reduction in time compression but preservation of phase compression of place field sequences within theta cycles, and (4) decrease of firing rates of both pyramidal cells and interneurons, commensurate with the increased duration of theta cycles.

MS cooling may nonspecifically affect several targets, including local neurons and their intraseptal interactions, as well as the transmitter release probability of subcortical neuromodulators terminating in MS, and it can also alter spike propagation in axons passing through the MS (Fee and Long, 2011; Volgushev et al., 2000). Our goal was not to disclose the local physiological effects of temperature manipulations in MS but to bring about a reliable macroscopic phenotype, theta frequency, and examine the circuit mechanisms responsible for such change in the hippocampus. Since the cooling method affects circuit components relatively homogeneously, it is an alternative or complementary tool to neuron-specific perturbations (Fee and Long, 2011; Fuhrmann et al., 2015; Lee et al., 1994; Vandecasteele et al., 2014; Zutshi et al., 2018). Many of the subcortical neuromodulatory and supramammillary effects are likely mediated by affecting MS neurons (Vertes and Kocsis, 1997). They may be responsible for altering theta power but less so theta frequency. Selective damage to MS cholinergic neurons reduces theta power several-fold without affecting theta frequency (Lee et al., 1994). Furthermore, pharmacological blockade of muscarinic cholinergic receptors does not alter the cross-correlation structure of neuron pairs, spatial properties of place cells, the predictability of spiking in individual place cells from peer activity, or the decodability of patterns of simultaneously recoded place cell spikes (Venditto et al., 2019). Conversely, optogenetic activation of MS GABAergic, but not cholinergic, neurons can tune theta frequency (Zutshi et al., 2018; Fuhrmann et al., 2015), suggesting that MS cooling exerted its theta temporal/phase effects mainly by affecting MS GABAergic neurons (Borhegyi et al., 2004; Hangya et al., 2009; Simon et al., 2006; Stewart and Fox, 1990; Zutshi et al., 2018). Thus, even if MS cooling affects multiple mechanisms, the strongest correlation between MS temperature and theta frequency oscillation suggests that MS GABAergic neurons are likely involved.

Please cite this article in press as: Petersen and Buzsáki, Cooling of Medial Septum Reveals Theta Phase Lag Coordination of Hippocampal Cell Assemblies, Neuron (2020), https://doi.org/10.1016/j.neuron.2020.05.023

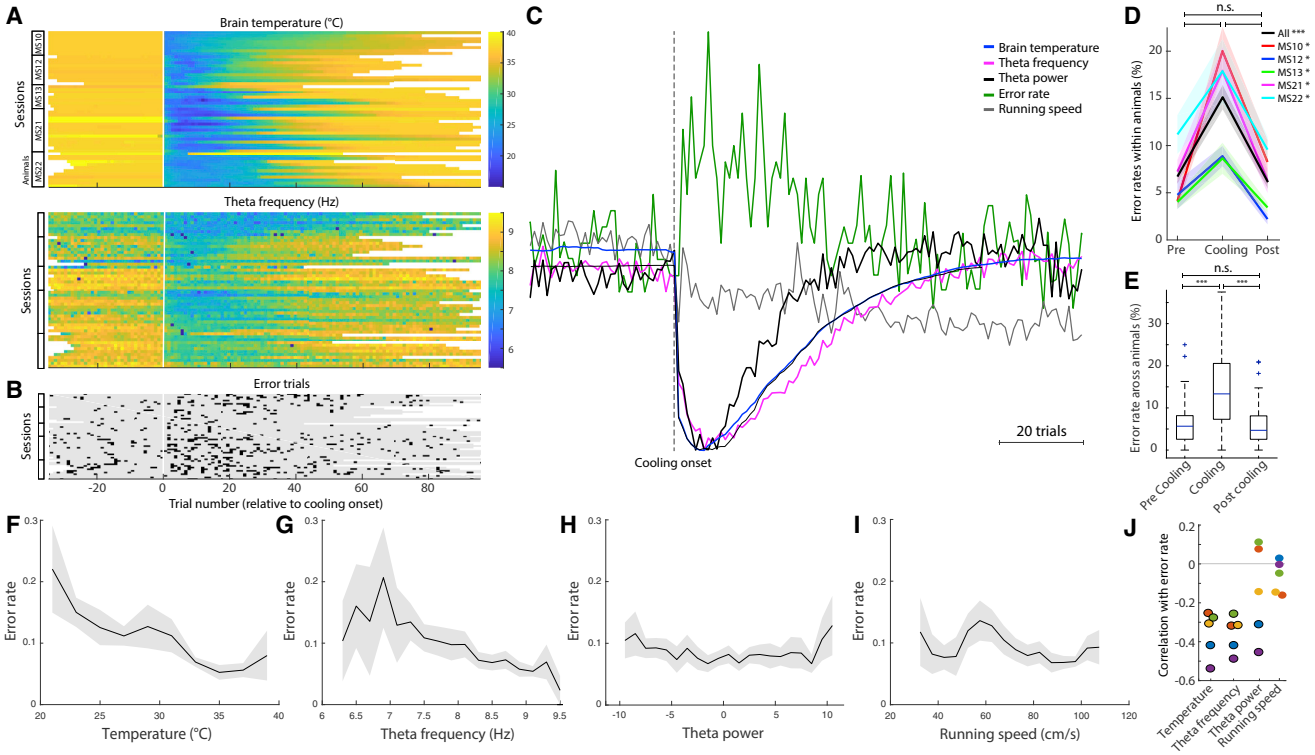

Figure 6. Effects of MS Cooling on Memory Performance

(A) MS temperature (top) and theta frequency shift (bottom) as a function of trial number (x axis). Each line corresponds to a single session. Animal IDs are indicated on the left. Vertical line marks the onset of cooling.

(B) Incidence of error trials in the same sessions.

(C) Time courses of MS temperature, theta frequency, power ,and running speed (mean of all sessions). Note tight correlation between MS temperature, theta frequency and power. In contrast, speed shows a monotonic function across trials.

(D) Choice errors shown separately for each animal. SEs are shown in shaded colors. Black line represents group means. *$p < 0.05$; ***$p = 10^{-6}$.

(E) Choice errors shown as boxplots constructed from all sessions. **$p < 10^{-7}$. n.s., nonsignificant.

(F–I) Relationship between memory errors and temperature (F), theta frequency (G), theta power (H), and running speed (I). SEs are shown in shaded colors (F–I).

(J) Correlation values between memory errors and parameters shown in (F)–(I) for each rat. Significant values are indicated by black circles ($p < 0.05$). Same color indicates the same animal.

Theta Phase Organization of Hippocampal Cell Assemblies

Early experiments suggested that the MS acts as a pacemaker, sending out synchronous outputs, akin to a conductor of an orchestra (Borhegyi et al., 2004; Buzsáki, 2002; Chadwick et al., 2016; Petsche et al., 1962; Stewart and Fox, 1990; Sweeney et al., 1992; Zutshi et al., 2018). An alternative model is based on the reciprocal relationship between MS and the hippocampus (Hangya et al., 2009). In one arm of the loop, MS GABAergic neurons innervate hippocampal and entorhinal interneurons (Freund and Antal, 1988; Fuchs et al., 2016; Gonzalez-Sulser et al., 2014; Takács et al., 2008; Unal et al., 2015). In the return direction, long-range GABAergic neurons send axons to the MS (Gulyás et al., 2003; Tóth et al., 1993). Our observations suggest that MS neurons work together with these long-range GABAergic hippocampo-septal, and likely entorhinal-septal, feedback neurons to provide theta phase coordination in the entire entorhinal-hippocampal system (Figure S6). Future experiments are needed to reveal whether MS cooling also affects theta phase delays along the septo-temporal axis of the hippocampus and whether there is a corresponding anatomical organization within the MS that may reflect such theta phase delays. Yet, the current findings provide important clues about how the MS contributes to theta phase space organization of hippocampal activity.

Interneurons, populations of pyramidal cells, and MS neurons all fire at the frequency of hippocampal LFP (Buzsáki, 2010; Geisler et al., 2010; Gothard et al., 1996). In contrast, active individual pyramidal cells and granule cells oscillate faster (f_p) than the population activity (f_{LFP}), resulting in phase interference and measured experimentally by the phase precession slope (O'Keefe and Recce, 1993). The difference between oscillation frequency of place cells and LFP theta is inversely correlated with place field size and affected by the running speed of the animal ($L_{PF} = v/(f_p - f_{LFP})$; Geisler et al., 2010). We found that at faster running velocities, the difference between f_p and f_{LFP} increased, which may explain the place field size invariance (Geisler et al., 2007; Huxter et al., 2003). These relationships were preserved during MS cooling, which can account for the

Please cite this article in press as: Petersen and Buzsáki, Cooling of Medial Septum Reveals Theta Phase Lag Coordination of Hippocampal Cell Assemblies, Neuron (2020), https://doi.org/10.1016/j.neuron.2020.05.023

place field size invariance and other spatial features of place cells during MS cooling. In contrast, a unidirectional MS-hippocampus command mechanism cannot explain the observed place field size preservation.

The magnitude of phase precession is often explained by the interference between the MS-driven LFP theta and the faster oscillation of place neurons (O'Keefe and Burgess, 2005; Burgess et al., 2007). Under the unidirectional pacemaker model, the slowing the output MS theta frequency would result in a larger $f_p - f_{LFP}$ difference and, consequently, steeper phase precession and smaller place fields, as suggested by a computational model (Chadwick et al., 2016). However, during MS cooling, f_p and f_{LFP} decreased proportionally (i.e., $f_p - f_{LFP}$ difference remained constant), and the influence of the rat's running velocity on f_p was preserved (Figures 4A and 4C). These preserved relationships can explain why place field size was not affected by MS cooling. Proportional slowing of f_p and f_{LFP} was also observed in a virtual reality experiment (Aghajan et al., 2015; Ravassard et al., 2013). Overall, these distinct approaches support the hypothesis that theta phase preservation of spikes is a fundamental mechanism in the hippocampal system.

Further support for the primacy of phase, as opposed to time, comes from the time lag comparisons of place cell spikes. The travel distances between the peak positions of place cell sequences (L_{tr}) are correlated with their theta-scale time lags (τ) and phase lags, and the ratio of travel distance and theta-scale time lag (L_{tr}/τ) is known as distance-to-time compression (*c;* Dragoi and Buzsáki, 2006; Maurer et al., 2012). This distance-to-duration compression is believed to be the mechanism that chains together evolving place cell assemblies within theta cycles (Chadwick et al., 2016; Dragoi and Buzsáki, 2006; Harris et al., 2002; Lisman and Jensen, 2013; Mehta et al., 2002; O'Keefe and Burgess, 2005; Pastalkova et al., 2008; Samsonovich and McNaughton, 1997; Skaggs et al., 1996; Wang et al., 2015). Neither place field sizes (L_{PF}) nor the distances between place field peaks (L_{tr}) were affected by MS cooling. On the other hand, the theta-scale time lags (τ) between successive place cell assemblies increased. As a result, the compression index (*c*) decreased. In contrast, phase lags between successive place cells within the theta cycle were not affected.

Theta phase organization is also reflected by the observed firing rate changes. During MS cooling, LFP theta frequency decreased by 12%, and within-field firing rates of place cells decreased by a similar proportion (12%; interneurons 14%). This relationship can explain why the fraction of place cells and the number of spikes within theta cycles were largely unaffected by MS manipulation. MS cooling, therefore, exerted its main physiological effect by dispersing the same number of cell assemblies within the phase space of the prolonged theta cycles (Figure 1B), as quantified by the longer τ in the face of preserved phase differences between place field peaks. Overall, these findings suggest that the fundamental organization of cell assemblies in the hippocampus is based on theta phase-preservation mechanisms, even at the expense of longer temporal lags between assemblies. In general, our results imply that the physiological operations of the hippocampus can be described mechanistically by its cycle-based organization and without reference to the concept of time (Buzsáki and Tingley, 2018).

Potential Mechanisms

What are the mechanisms that keep the phase-organization within the MS-hippocampus loop when theta frequency changes? A previous experimental-computational model has shown that temporal lags between assemblies (τ) are correlated with the duration of the theta cycle (Geisler et al., 2010). It was hypothesized that the mechanism responsible for the delays between cells assemblies is inhibition in local hippocampal circuits (Geisler et al., 2010). However, the current findings demonstrate that the MS plays a critical role in adjusting the theta phase delays between neighboring place fields of pyramidal cells. In addition, previous findings indicate that following pharmacological inactivation of the MS, internally generated sequences disappear and theta-scale timing of place cells is impaired without affecting place cell positions in the maze (Wang et al., 2015). A putative mechanism may involve the reciprocal circuit between GABAergic neurons in MS and hippocampus (Figure S6). MS parvalbumin-expressing neurons innervate a variety of inhibitory neuron types in the hippocampus (Freund and Antal, 1988) and entorhinal cortex (Fuchs et al., 2016; Gonzalez-Sulser et al., 2014; Jeffery et al., 1995; Justus et al., 2017; Viney et al., 2018), while cholinergic neurons affect both principal cells and interneurons (Unal et al., 2015). In turn, long-range hippocampo-septal interneurons inhibit MS neurons (Gulyás et al., 2003; Takács et al., 2008; Tóth et al., 1993). These hippocampo-septal inhibitory neurons are likely of special importance, because they are the best candidate for integrating the activity of multiple place cell assemblies and feedback population theta-oscillatory pulsing to subgroups of MS neurons.

MS-Cooling-Induced Memory Impairment

MS cooling exerted a robust effect on spatial memory, comparable to damage or pharmacologic inactivation of MS (Bolding et al., 2020; Chang and Gold, 2004; Chrobak et al., 1989; Givens and Olton, 1990; Winson, 1978). Choice errors correlated best with the temporal dynamic of MS cooling. Whether memory impairment is due to the documented physiological changes in the hippocampus or other mechanisms remains an open question.

In addition to MS neurons, our manipulation may have affected septal afferents, fibers of passage, and possibly their surrounding structures. Therefore, one possible interpretation of the behavioral effects is that moderate cooling of lateral septum, the nucleus accumbens and/or anterior end of the hippocampus is responsible for the behavioral deficit. However, lesion of lateral septum does not have an impact on spatial behavior (Fraser et al., 1991; Galey et al., 1985; Leutgeb and Mizumori, 1999; Winson, 1978). Electrolytic lesions (Thifault et al., 1998) or ibotenic-acid-induced lesions (Annett et al., 1989) of the nucleus accumbens did not impair spatial behavior and, in fact, damaging catecholaminergic terminals selectively in the n. accumbens slightly improved spatial alternation (Taghzouti et al., 1985). Fibers of passage of subcortical neuromodulator neurons through the medial or lateral septum typically affect spontaneous alternation via the MS (Lalonde, 2002).

In our experiments, memory errors reached maximum tens of seconds before mild cooling was observed in the hippocampus, suggesting that this mild secondary effect cannot explain

memory impairment. Importantly, previous studies have shown that decreasing brain temperature even down to 30°C was not sufficient to impair spatial navigation in rats (Andersen and Moser, 1995; Moser and Andersen, 1994). In humans, cognitive functions are not affected until the brain is cooled to ~33°C (Fay and Smith, 1941). Thus, while we cannot exclude impaired spike transmission of fibers of passage in the MS as a contributing factor, moderate cooling of the structures surrounding the MS may not fully account for the observed severe memory deficit. The moderate firing rate decrease of hippocampal neurons remains a candidate for the behavioral errors.

A remaining potential explanation is that the seemingly subtle but multiple changes of physiological parameters in the hippocampus (and expected but unobserved parallel changes in the entorhinal cortex) were responsible for the memory deficit. This possibility is supported by the observation that the temporal dynamic of choice errors correlated best with the time course of theta frequency decrease and that the maximum error rates occurred tens of seconds before a slight temperature decrease was detected in the hippocampus. Similarly, intra-MS infusion of the tetracaine, muscimol, and scopolamine suppressed theta oscillations and impaired performance in a spatial alternation task, and the choice errors best correlated with a change in theta oscillation frequency (Givens and Olton, 1990). During MS cooling, the same segment of the environment was "represented" by the same number of neuronal assemblies, but the time offsets between successive assemblies were longer in each theta cycle. Therefore, a possible explanation for the memory impairment, despite preserved spatial features of place cells, is that downstream reader structures, presumably not part of the MS-controlled theta system, failed to interpret the temporally altered hippocampal messages (Robbe and Buzsáki, 2009; but see Venditto et al., 2019). Overall, our findings suggest that the fundamental organization scheme in the septo-hippocampal system is phase based and that even minuscule temporal changes in large interconnected circuits may have behavioral consequences.

STAR★METHODS

Detailed methods are provided in the online version of this paper and include the following:

- KEY RESOURCES TABLE
- RESOURCE AVAILABILITY
  - Lead Contact
  - Materials Availability
  - Data and Code Availability
- EXPERIMENTAL MODEL AND SUBJECT DETAILS
  - Subjects and surgery
- METHOD DETAILS
  - Cooling devices
  - Dry ice cryoprobe
  - Peltier cooling device
  - Electrophysiological Recordings
  - Memory-demanding alternation task in a theta maze
- QUANTIFICATION AND STATISTICAL ANALYSIS
  - Spike Sorting
  - Unit Classification
  - Theta phase and phase precession
  - Oscillation Frequency of Neurons
  - Place cell analysis
  - Spatial temporal compression
  - Statistical Analyses

SUPPLEMENTAL INFORMATION

Supplemental Information can be found online at https://doi.org/10.1016/j.neuron.2020.05.023.

ACKNOWLEDGMENTS

We would like to thank Andrew Maurer, Viktor Varga, Manuel Valero, and Antonio Fernandez-Ruiz for helpful comments on the manuscript. This work was supported by the Independent Research Fund Denmark (grant DFF-5053-00279), Lundbeckfonden (grant R271-2017-1687), the NIH (grants MH122391, MH54671, and MH107396), the NSF (NeuroNex grant 1707316), and grants NIH U19 NS107616 and U19 NS104590.

AUTHOR CONTRIBUTIONS

G.B. and P.C.P. designed the experiments. P.C.P. performed the experiments and analyzed data. G.B. and P.C.P. wrote the paper.

DECLARATION OF INTERESTS

The authors declare no competing interests.

Received: March 25, 2020
Revised: April 26, 2020
Accepted: May 16, 2020
Published: June 10, 2020

REFERENCES

Aghajan, Z.M., Acharya, L., Moore, J.J., Cushman, J.D., Vuong, C., and Mehta, M.R. (2015). Impaired spatial selectivity and intact phase precession in two-dimensional virtual reality. Nat. Neurosci. *18*, 121–128.

Andersen, P., and Moser, E.I. (1995). Brain temperature and hippocampal function. Hippocampus *5*, 491–498.

Annett, L.E., McGregor, A., and Robbins, T.W. (1989). The effects of ibotenic acid lesions of the nucleus accumbens on spatial learning and extinction in the rat. Behav. Brain Res. *31*, 231–242.

Aronov, D., and Fee, M.S. (2011). Analyzing the dynamics of brain circuits with temperature: design and implementation of a miniature thermoelectric device. J. Neurosci. Methods *197*, 32–47.

Bolding, K.A., Ferbinteanu, J., Fox, S.E., and Muller, R.U. (2020). Place cell firing cannot support navigation without intact septal circuits. Hippocampus *30*, 175–191.

Borhegyi, Z., Varga, V., Szilágyi, N., Fabo, D., and Freund, T.F. (2004). Phase segregation of medial septal GABAergic neurons during hippocampal theta activity. J. Neurosci. *24*, 8470–8479.

Brandon, M.P., Bogaard, A.R., Libby, C.P., Connerney, M.A., Gupta, K., and Hasselmo, M.E. (2011). Reduction of theta rhythm dissociates grid cell spatial periodicity from directional tuning. Science *332*, 595–599.

Burgess, N., Barry, C., and O'Keefe, J. (2007). An oscillatory interference model of grid cell firing. Hippocampus *17*, 801–812.

Buzsáki, G. (2002). Theta oscillations in the hippocampus. Neuron *33*, 325–340.

Buzsáki, G. (2010). Neural syntax: cell assemblies, synapsembles, and readers. Neuron *68*, 362–385.

Buzsáki, G., Czopf, J., Kondákor, I., and Kellényi, L. (1986). Laminar distribution of hippocampal rhythmic slow activity (RSA) in the behaving rat: current-source density analysis, effects of urethane and atropine. Brain Res. *365*, 125–137.

Buzsáki, G., and Tingley, D. (2018). Space and Time: The Hippocampus as a Sequence Generator. Trends Cogn. Sci. *22*, 853–869.

Chadwick, A., van Rossum, M.C., and Nolan, M.F. (2016). Flexible theta sequence compression mediated via phase precessing interneurons. eLife *5*, e20349.

Chang, Q., and Gold, P.E. (2004). Impaired and spared cholinergic functions in the hippocampus after lesions of the medial septum/vertical limb of the diagonal band with 192 IgG-saporin. Hippocampus *14*, 170–179.

Chrobak, J.J., Stackman, R.W., and Walsh, T.J. (1989). Intraseptal administration of muscimol produces dose-dependent memory impairments in the rat. Behav. Neural Biol. *52*, 357–369.

Czurkó, A., Hirase, H., Csicsvari, J., and Buzsáki, G. (1999). Sustained activation of hippocampal pyramidal cells by 'space clamping' in a running wheel. Eur. J. Neurosci. *11*, 344–352.

Dannenberg, H., Kelley, C., Hoyland, A., Monaghan, C.K., and Hasselmo, M.E. (2019). The firing rate speed code of entorhinal speed cells differs across behaviorally relevant time scales and does not depend on medial septum inputs. J. Neurosci. *39*, 3434–3453.

Diba, K., and Buzsáki, G. (2008). Hippocampal network dynamics constrain the time lag between pyramidal cells across modified environments. J. Neurosci. *28*, 13448–13456.

Dragoi, G., and Buzsáki, G. (2006). Temporal encoding of place sequences by hippocampal cell assemblies. Neuron *50*, 145–157.

English, D.F., McKenzie, S., Evans, T., Kim, K., Yoon, E., and Buzsáki, G. (2017). Pyramidal Cell-Interneuron Circuit Architecture and Dynamics in Hippocampal Networks. Neuron *96*, 505–520.

Fay, T., and Smith, G.W. (1941). Observations on reflex responses during prolonged periods of human refrigeration. Arch. Neurol. Psychiatry *45*, 215–222.

Fee, M.S., and Long, M.A. (2011). New methods for localizing and manipulating neuronal dynamics in behaving animals. Curr. Opin. Neurobiol. *21*, 693–700.

Fraser, K.A., Poucet, B., Partlow, G., and Herrmann, T. (1991). Role of the medial and lateral septum in a variable goal spatial problem solving task. Physiol. Behav. *50*, 739–744.

Freund, T.F., and Antal, M. (1988). GABA-containing neurons in the septum control inhibitory interneurons in the hippocampus. Nature *336*, 170–173.

Fuchs, E.C., Neitz, A., Pinna, R., Melzer, S., Caputi, A., and Monyer, H. (2016). Local and distant input controlling excitation in layer II of the medial entorhinal cortex. Neuron *89*, 194–208.

Fuhrmann, F., Justus, D., Sosulina, L., Kaneko, H., Beutel, T., Friedrichs, D., Schoch, S., Schwarz, M.K., Fuhrmann, M., and Remy, S. (2015). Locomotion, theta oscillations, and the speed-correlated firing of hippocampal neurons are controlled by a medial septal glutamatergic circuit. Neuron *86*, 1253–1264.

Galey, D., Durkin, T., Sifakis, G., Kempf, E., and Jaffard, R. (1985). Facilitation of spontaneous and learned spatial behaviours following 6-hydroxydopamine lesions of the lateral septum: a cholinergic hypothesis. Brain Res. *340*, 171–174.

Geisler, C., Robbe, D., Zugaro, M., Sirota, A., and Buzsáki, G. (2007). Hippocampal place cell assemblies are speed-controlled oscillators. Proc. Natl. Acad. Sci. USA *104*, 8149–8154.

Geisler, C., Diba, K., Pastalkova, E., Mizuseki, K., Royer, S., and Buzsáki, G. (2010). Temporal delays among place cells determine the frequency of population theta oscillations in the hippocampus. Proc. Natl. Acad. Sci. USA *107*, 7957–7962.

Giocomo, L.M., Zilli, E.A., Fransén, E., and Hasselmo, M.E. (2007). Temporal frequency of subthreshold oscillations scales with entorhinal grid cell field spacing. Science *315*, 1719–1722.

Givens, B.S., and Olton, D.S. (1990). Cholinergic and GABAergic modulation of medial septal area: effect on working memory. Behav. Neurosci. *104*, 849–855.

Gonzalez-Sulser, A., Parthier, D., Candela, A., McClure, C., Pastoll, H., Garden, D., Sürmeli, G., and Nolan, M.F. (2014). GABAergic projections from the medial septum selectively inhibit interneurons in the medial entorhinal cortex. J. Neurosci. *34*, 16739–16743.

Gothard, K.M., Skaggs, W.E., and McNaughton, B.L. (1996). Dynamics of mismatch correction in the hippocampal ensemble code for space: interaction between path integration and environmental cues. J. Neurosci. *16*, 8027–8040.

Gulyás, A.I., Hájos, N., Katona, I., and Freund, T.F. (2003). Interneurons are the local targets of hippocampal inhibitory cells which project to the medial septum. Eur. J. Neurosci. *17*, 1861–1872.

Hafting, T., Fyhn, M., Bonnevie, T., Moser, M.-B., and Moser, E.I. (2008). Hippocampus-independent phase precession in entorhinal grid cells. Nature *453*, 1248–1252.

Hangya, B., Borhegyi, Z., Szilágyi, N., Freund, T.F., and Varga, V. (2009). GABAergic neurons of the medial septum lead the hippocampal network during theta activity. J. Neurosci. *29*, 8094–8102.

Harris, K.D., Henze, D.A., Hirase, H., Leinekugel, X., Dragoi, G., Czurkó, A., and Buzsáki, G. (2002). Spike train dynamics predicts theta-related phase precession in hippocampal pyramidal cells. Nature *417*, 738–741.

Harris, K.D., Csicsvari, J., Hirase, H., Dragoi, G., and Buzsáki, G. (2003). Organization of cell assemblies in the hippocampus. Nature *424*, 552–556.

Harvey, C.D., Collman, F., Dombeck, D.A., and Tank, D.W. (2009). Intracellular dynamics of hippocampal place cells during virtual navigation. Nature *461*, 941–946.

Huxter, J., Burgess, N., and O'Keefe, J. (2003). Independent rate and temporal coding in hippocampal pyramidal cells. Nature *425*, 828–832.

Jeffery, K.J., Donnett, J.G., and O'Keefe, J. (1995). Medial septal control of theta-correlated unit firing in the entorhinal cortex of awake rats. Neuroreport *6*, 2166–2170.

Justus, D., Dalügge, D., Bothe, S., Fuhrmann, F., Hannes, C., Kaneko, H., Friedrichs, D., Sosulina, L., Schwarz, I., Elliott, D.A., et al. (2017). Glutamatergic synaptic integration of locomotion speed via septoentorhinal projections. Nat. Neurosci. *20*, 16–19.

Kamondi, A., Acsády, L., Wang, X.J., and Buzsáki, G. (1998). Theta oscillations in somata and dendrites of hippocampal pyramidal cells in vivo: activity-dependent phase-precession of action potentials. Hippocampus *8*, 244–261.

Katz, P.S., Sakurai, A., Clemens, S., and Davis, D. (2004). Cycle period of a network oscillator is independent of membrane potential and spiking activity in individual central pattern generator neurons. J. Neurophysiol. *92*, 1904–1917.

Kay, K., Chung, J.E., Sosa, M., Schor, J.S., Karlsson, M.P., Larkin, M.C., Liu, D.F., and Frank, L.M. (2020). Constant sub-second cycling between representations of possible futures in the hippocampus. Cell *180*, 552–567.e25.

Kjelstrup, K.B., Solstad, T., Brun, V.H., Hafting, T., Leutgeb, S., Witter, M.P., Moser, E.I., and Moser, M.-B. (2008). Finite scale of spatial representation in the hippocampus. Science *321*, 140–143.

Lalonde, R. (2002). The neurobiological basis of spontaneous alternation. Neurosci. Biobehav. Rev. *26*, 91–104.

Lee, M.G., Chrobak, J.J., Sik, A., Wiley, R.G., and Buzsáki, G. (1994). Hippocampal theta activity following selective lesion of the septal cholinergic system. Neuroscience *62*, 1033–1047.

Leutgeb, S., and Mizumori, S.J.Y. (1999). Excitotoxic septal lesions result in spatial memory deficits and altered flexibility of hippocampal single-unit representations. J. Neurosci. *19*, 6661–6672.

Lisman, J.E., and Jensen, O. (2013). The θ-γ neural code. Neuron *77*, 1002–1016.

Long, M.A., and Fee, M.S. (2008). Using temperature to analyse temporal dynamics in the songbird motor pathway. Nature *456*, 189–194.

Lubenov, E.V., and Siapas, A.G. (2009). Hippocampal theta oscillations are travelling waves. Nature *459*, 534–539.

Maurer, A.P., Cowen, S.L., Burke, S.N., Barnes, C.A., and McNaughton, B.L. (2006). Organization of hippocampal cell assemblies based on theta phase precession. Hippocampus *16*, 785–794.

Maurer, A.P., Burke, S.N., Lipa, P., Skaggs, W.E., and Barnes, C.A. (2012). Greater running speeds result in altered hippocampal phase sequence dynamics. Hippocampus *22*, 737–747.

McNaughton, B.L., Barnes, C.A., and O'Keefe, J. (1983). The contributions of position, direction, and velocity to single unit activity in the hippocampus of freely-moving rats. Exp. Brain Res. *52*, 41–49.

McNaughton, N., Ruan, M., and Woodnorth, M.-A. (2006). Restoring theta-like rhythmicity in rats restores initial learning in the Morris water maze. Hippocampus *16*, 1102–1110.

Mehta, M.R., Lee, A.K., and Wilson, M.A. (2002). Role of experience and oscillations in transforming a rate code into a temporal code. Nature *417*, 741–746.

Mizuseki, K., Sirota, A., Pastalkova, E., and Buzsáki, G. (2009). Theta oscillations provide temporal windows for local circuit computation in the entorhinal-hippocampal loop. Neuron *64*, 267–280.

Mizuseki, K., Diba, K., Pastalkova, E., and Buzsáki, G. (2011). Hippocampal CA1 pyramidal cells form functionally distinct sublayers. Nat. Neurosci. *14*, 1174–1181.

Montgomery, S.M., Betancur, M.I., and Buzsáki, G. (2009). Behavior-dependent coordination of multiple theta dipoles in the hippocampus. J. Neurosci. *29*, 1381–1394.

Moser, E.I., and Andersen, P. (1994). Conserved spatial learning in cooled rats in spite of slowing of dentate field potentials. J. Neurosci. *14*, 4458–4466.

Muller, R.U., and Kubie, J.L. (1989). The firing of hippocampal place cells predicts the future position of freely moving rats. J. Neurosci. *9*, 4101–4110.

O'Keefe, J., and Burgess, N. (2005). Dual phase and rate coding in hippocampal place cells: theoretical significance and relationship to entorhinal grid cells. Hippocampus *15*, 853–866.

O'Keefe, J., and Nadel, L. (1978). The Hippocampus as a Cognitive Map (Clarendon Press).

O'Keefe, J., and Recce, M.L. (1993). Phase relationship between hippocampal place units and the EEG theta rhythm. Hippocampus *3*, 317–330.

Pachitariu, M., Steinmetz, N.A., Kadir, S.N., Carandini, M., and Harris, K.D. (2016). Fast and accurate spike sorting of high-channel count probes with KiloSort. In Advances in Neural Information Processing Systems 29, D.D. Lee, M. Sugiyama, U.V. Luxburg, I. Guyon, and R. Garnett, eds. (Curran Associates), pp. 4448–4456.

Pastalkova, E., Itskov, V., Amarasingham, A., and Buzsáki, G. (2008). Internally generated cell assembly sequences in the rat hippocampus. Science *321*, 1322–1327.

Patel, J., Fujisawa, S., Berényi, A., Royer, S., and Buzsáki, G. (2012). Traveling theta waves along the entire septotemporal axis of the hippocampus. Neuron *75*, 410–417.

Petersen, P.C., and Buzsáki, G. (2020). CellExplorer: a graphical user interface and standardized pipeline for visualizing and characterizing single neuron features. bioRxiv. https://doi.org/10.1101/2020.05.07.083436.

Petersen, P.C., Hernandez, M., and Buzsáki, G. (2018). Public electrophysiological datasets collected in the Buzsaki Lab. https://buzsakilab.com/wp/public-data/. http://doi.org/10.5281/zenodo.3629881 (Zenodo).

Petersen, P.C., Watson, B., and Peyrache, A. (2020). KiloSortWrapper. https://github.com/petersenpeter/KilosortWrapper. http://doi.org/10.5281/zenodo.3604165 (Zenodo).

Petsche, H., Stumpf, C., and Gogolak, G. (1962). [The significance of the rabbit's septum as a relay station between the midbrain and the hippocampus. I. The control of hippocampus arousal activity by the septum cells]. Electroencephalogr. Clin. Neurophysiol. *14*, 202–211.

Ravassard, P., Kees, A., Willers, B., Ho, D., Aharoni, D.A., Cushman, J., Aghajan, Z.M., and Mehta, M.R. (2013). Multisensory control of hippocampal spatiotemporal selectivity. Science *340*, 1342–1346.

Robbe, D., and Buzsáki, G. (2009). Alteration of theta timescale dynamics of hippocampal place cells by a cannabinoid is associated with memory impairment. J. Neurosci. *29*, 12597–12605.

Royer, S., Sirota, A., Patel, J., and Buzsáki, G. (2010). Distinct representations and theta dynamics in dorsal and ventral hippocampus. J. Neurosci. *30*, 1777–1787.

Samsonovich, A., and McNaughton, B.L. (1997). Path integration and cognitive mapping in a continuous attractor neural network model. J. Neurosci. *17*, 5900–5920.

Simon, A.P., Poindessous-Jazat, F., Dutar, P., Epelbaum, J., and Bassant, M.-H. (2006). Firing properties of anatomically identified neurons in the medial septum of anesthetized and unanesthetized restrained rats. J. Neurosci. *26*, 9038–9046.

Skaggs, W.E., McNaughton, B.L., Wilson, M.A., and Barnes, C.A. (1996). Theta phase precession in hippocampal neuronal populations and the compression of temporal sequences. Hippocampus *6*, 149–172.

Stewart, M., and Fox, S.E. (1990). Do septal neurons pace the hippocampal theta rhythm? Trends Neurosci. *13*, 163–168.

Sweeney, J.E., Lamour, Y., and Bassant, M.H. (1992). Arousal-dependent properties of medial septal neurons in the unanesthetized rat. Neuroscience *48*, 353–362.

Taghzouti, K., Louilot, A., Herman, J.P., Le Moal, M., and Simon, H. (1985). Alternation behavior, spatial discrimination, and reversal disturbances following 6-hydroxydopamine lesions in the nucleus accumbens of the rat. Behav. Neural Biol. *44*, 354–363.

Takács, V.T., Freund, T.F., and Gulyás, A.I. (2008). Types and synaptic connections of hippocampal inhibitory neurons reciprocally connected with the medial septum. Eur. J. Neurosci. *28*, 148–164.

Thifault, S., Krémarik, P., and Lalonde, R. (1998). Effects of bilateral electrolytic lesions of the medial nucleus accumbens on exploration and spatial learning. Arch. Physiol. Biochem. *106*, 297–307.

Thompson, S.M., Masukawa, L.M., and Prince, D.A. (1985). Temperature dependence of intrinsic membrane properties and synaptic potentials in hippocampal CA1 neurons in vitro. J. Neurosci. *5*, 817–824.

Tóth, K., Borhegyi, Z., and Freund, T.F. (1993). Postsynaptic targets of GABAergic hippocampal neurons in the medial septum-diagonal band of broca complex. J. Neurosci. *13*, 3712–3724.

Tsanov, M. (2017). Speed and oscillations: medial septum integration of attention and navigation. Front. Syst. Neurosci. *11*, 67.

Unal, G., Joshi, A., Viney, T.J., Kis, V., and Somogyi, P. (2015). Synaptic targets of medial septal projections in the hippocampus and extrahippocampal cortices of the mouse. J. Neurosci. *35*, 15812–15826.

Vandecasteele, M., M, S., Royer, S., Belluscio, M., Berényi, A., Diba, K., Fujisawa, S., Grosmark, A., Mao, D., Mizuseki, K., et al. (2012). Large-scale recording of neurons by movable silicon probes in behaving rodents. J. Vis. Exp. *61*, e3568.

Vandecasteele, M., Varga, V., Berényi, A., Papp, E., Barthó, P., Venance, L., Freund, T.F., and Buzsáki, G. (2014). Optogenetic activation of septal cholinergic neurons suppresses sharp wave ripples and enhances theta oscillations in the hippocampus. Proc. Natl. Acad. Sci. USA *111*, 13535–13540.

Venditto, S.J.C., Le, B., and Newman, E.L. (2019). Place cell assemblies remain intact, despite reduced phase precession, after cholinergic disruption. Hippocampus *29*, 1075–1090.

Vertes, R.P., and Kocsis, B. (1997). Brainstem-diencephalo-septohippocampal systems controlling the theta rhythm of the hippocampus. Neuroscience *81*, 893–926.

Viney, T.J., Salib, M., Joshi, A., Unal, G., Berry, N., and Somogyi, P. (2018). Shared rhythmic subcortical GABAergic input to the entorhinal cortex and presubiculum. eLife *7*, e34395.

Volgushev, M., Vidyasagar, T.R., Chistiakova, M., Yousef, T., and Eysel, U.T. (2000). Membrane properties and spike generation in rat visual cortical cells during reversible cooling. J. Physiol. *522*, 59–76.

Wang, Y., Romani, S., Lustig, B., Leonardo, A., and Pastalkova, E. (2015). Theta sequences are essential for internally generated hippocampal firing fields. Nat. Neurosci. *18*, 282–288.

Winson, J. (1978). Loss of hippocampal theta rhythm results in spatial memory deficit in the rat. Science *201*, 160–163.

Zutshi, I., Brandon, M.P., Fu, M.L., Donegan, M.L., Leutgeb, J.K., and Leutgeb, S. (2018). Hippocampal neural circuits respond to optogenetic pacing of theta frequencies by generating accelerated oscillation frequencies. Curr. Biol. *28*, 1179–1188.e3.

Please cite this article in press as: Petersen and Buzsáki, Cooling of Medial Septum Reveals Theta Phase Lag Coordination of Hippocampal Cell Assemblies, Neuron (2020), https://doi.org/10.1016/j.neuron.2020.05.023

STAR★METHODS

KEY RESOURCES TABLE

REAGENT or RESOURCE	SOURCE	IDENTIFIER
Subjects: Long-Evans rats (9 male adults)	Charles River	Cat#: Crl:LE 006
Hippocampal data (Public data share with data from our lab)	Peter C. Petersen & Gyorgy Buzsaki	https://buzsakilab.com/wp/public-data/
CellExplorer (Cell classification pipeline and graphical interface)	Peter C. Petersen & Gyorgy Buzsaki	http://cellexplorer.org
KiloSort (Template based spike sorting MATLAB software)	Pachitariu M & Cortex-lab	https://github.com/cortex-lab/KiloSort
KilosortWrapper (A wrapper for KiloSort written in MATLAB)	Peter C. Petersen & Brendon Watson	https://github.com/petersenpeter/KilosortWrapper
Phy (Python GUI for manual spike curation)	Cyrille Rossant, Ken Harris et al.	https://github.com/cortex-lab/phy
Phy plugins	Peter C. Petersen	https://github.com/petersenpeter/phy-plugins
MATLAB	MathWorks	https://www.mathworks.com
Buzcode (MATLAB analysis tools)	Buzsaki Lab	https://github.com/buzsakilab/buzcode
FMA Toolbox (MATLAB toolbox for Freely Moving Animal (FMA))	Michaël Zugaro	https://fmatoolbox.sourceforge.net
Silicon probe (5x12, 6x10)	NeuroNexus	https://neuronexus.com
Silicon probe (4x16)	Cambridge Neurotech	https://www.cambridgeneurotech.com
Intan RHD2000 (recording equipment)	Intan technologies	https://intantech.com/RHD_USB_interface_board.html

RESOURCE AVAILABILITY

Lead Contact

Further information and requests for resources and reagents should be directed to and will be fulfilled by the Lead Contact, György Buzsáki (gyorgy.buzsaki@nyulangone.org)

Materials Availability

This study did not generate new unique reagents.

Data and Code Availability

The dataset will be available from our data share via our website https://buzsakilab.com/wp/public-data/ (Petersen et al., 2018) and will be uploaded to CRCNS.org. The code that support the findings of this study will be made available from the corresponding author upon reasonable request.

EXPERIMENTAL MODEL AND SUBJECT DETAILS

Subjects and surgery

Rats (adult male Long-Evans, 250-450 g, 3-6 months old) were kept in a vivarium on a 12-hour light/dark cycle and were housed 2 per cage before surgery and individually after it. All experiments were approved by the Institutional Animal Care and Use Committee at New York University Medical Center.

Animals were anesthetized with isoflurane anesthesia and craniotomies were performed under stereotaxic guidance. A custom designed 3D printed cap (Figure S1A) was attached to the skull with meta-bond, serving as a base for the probe implants and protection. A 12cm x 12cm sheet of copper mesh had beforehand been attached with dental cement to the base, from which a Faraday box/protector cap was later formed. Rats (Table S1) were implanted with silicon probes and tungsten wires to record local field potential (LFP) and spikes from the CA1 pyramidal layer (Vandecasteele et al., 2014). The tip of the cooling device was implanted at AP: +0.8mm, ML: 0.6mm (tilted 6° toward the midline), and lowered 6 mm below the brain surface, after which it was attached to the skull and base.

Silicon probes (NeuroNexus, Ann-Arbor, MI and Cambridge Neurotech, Cambridge, UK) were implanted in the dorsal hippocampus (antero-posterior (AP) −3.5mm from Bregma and 2.5 mm from the midline along the medial-lateral axis (ML)). The silicon probes

consisted of three designs (table q): 4-shank with 16 sites per shank in a poly 3 staggered configuration, 5-shank with 12 sites each shank in a staggered configuration, and 6-shank probe with 10 sites per shank (Figure 2B). They were mounted on custom-made micro-drives (Figure S1E) to allow their precise vertical movement after implantation (Vandecasteele et al., 2012). Probes were implanted above the target region by attaching the micro-drives to the skull with dental cement (Figure S1E). Craniotomies were sealed with sterile wax or gel. Stainless steel screws or 100μm steel wires were bilaterally screwed or implanted above the cerebellum, serving as ground and reference electrodes, respectively, for electrophysiological recordings (Figure S1E). At the end of electrode implantation and cryoprobe implantation (see below), the copper mesh was folded upward, connected to the ground screw, and painted with dental cement. The mesh acts as a Faraday cage, shielding the recordings from environmental electric noise and muscle artifacts, provides structural stability and keep debris away from the probe implants. After post-surgery recovery, probes were moved gradually in 50 μm to 150 μm steps until they reached the CA1 the pyramidal layer. The pyramidal layer of the CA1 region was identified by physiological markers: increased unit activity, strong theta oscillations and phase reversal of the sharp wave ripple oscillations (Mizuseki et al., 2011).

METHOD DETAILS

Cooling devices

Two different cooling techniques were used. A Peltier device and dry ice in Styrofoam chamber ('dry ice cryoprobe'). Both cooling devices were attached to a silver wire that conducted the cooling to the medial septum (Figure 2A).

Dry ice cryoprobe

A 15mm diameter 3D printed container with lid was constructed and a hollow cylinder made from Styrofoam (outer diameter: 18mm, inner diameter: 10mm; thermal conductivity: 0.03 W/m) was inserted into the container. A 20 mm silver wire (127μm diameter, a-m systems, #781500; thermal conductivity: 406.0 W/mK), wrapped with graphene sheet (graphene-supermarket: Conductive Graphene Sheets, thickness: 25μm; thermal conductivity: 1300-1500W/m in x-y plane and 13-15W/m in z plane), was inserted through the base of the Styrofoam container and attached to the inside of the chamber with thermal adhesive (Arctic Silver Thermal Adhesive, ASTA-7G; thermal conductivity: > 7.5W/m-K). 10mm of the wire was protruding from the base of the chamber. The protruding silver wire was then inserted into an 8 mm long hollow polyimide tube (1.1 mm diameter, Cole-Parmer 95820-09), such that 1.5mm of the silver wire was exposed. The polyimide tube was further sealed with adhesive in both ends to create a contained air insulation around the silver wire (Figure 2A). The air insulation served as a thermal insulation (thermal conductivity: 0.024), to minimize the cooling effects along the wire (Aronov and Fee, 2011). Finally, a thermocouple (a temperature sensor: Omega, 80μm wires, product number 5SC-TT-K-40-72) was attached with epoxy adhesive to the cooling implant with the tip of the probe aligned with the protruding silver wire (Figures 2A and S1A). Cooling with dry ice was achieved by placing a small amount of dry ice into the ''cooling chamber,'' which conducted the cooling to the exposed implanted silver wire.

Peltier cooling device

The hot side of a two-stage Peltier device (custom thermoelectric, 04812-5L31-04CFG 2 Stage Thermoelectric/Peltier Module) was attached to a copper heatsink (5mm x 5 mm, Enzotech MOS-C10 Forged Copper MOSFET Heatsinks) with heat-conductive adhesive (Arctic Silver, Arctic Silver Thermal Adhesive). The heatsink was shaped to fit the inner dimensions of a 25 mm x 25 mm electric fan (GDSTIME, 5V DC Brushless fan). An 18 mm long silver wire (200μm diameter, a-m systems #782000) was attached to the cold side of the peltier device with heat conductive adhesive. An 8 mm long polyimide tube (1.1 mm diameter, Cole-Parmer 95820-09) was attached around the silver wire, sealed, and a thermocouple temperature sensor (Omega, 80μm wires, product number 5SC-TT-K-40-72) was attached to the tube. 1.5mm of the silver wire was exposed at the tip of the cooling device.

Electrophysiological Recordings

Animals were handled daily and accommodated to the experimenter before surgery. They were water restricted for 22 hours and trained to perform the behavioral task prior to surgery. After recovery from surgery, the animals were water restricted again to perform a spatial alternation task in a 'theta' (Figure 8-shape) maze. The behavior session typically lasted 40 min, consisting of 40 control trials, after which the cooling was applied by manually placing a small amount of dry ice in the cooling chamber. The cooling typically peaked after about 60 s after the cooling onset (Figure S1G) and lasted for about 10-12 minutes, corresponding to approximately 50 trials (Figures 6C and S2). The animal would continue the task for a total number of trials ranging from 80 to 200 (mean: 150 trials). The behavior was preceded and followed by 1-3 hours sleep sessions in the home cage of the rat.

Memory-demanding alternation task in a theta maze

In a 'theta' (Figure 8-shape) maze (110 cm diameter, Figure 2C), animals were trained to alternate between the left and the right arms to receive water drops at the reward locations (Figure 2C). The maze was placed on a platform 1 m above the floor. The rat started from the reward location, ran along the central arm, after which it chose to run along the left or the right arm. If the animal performed the alternation correctly (visited the opposite arm than they visited in the previous trial), it received water reward. If it chose the wrong direction, the path to the reward location was blocked and the rat was forced to run back along the correct arm to collect reward.

Please cite this article in press as: Petersen and Buzsáki, Cooling of Medial Septum Reveals Theta Phase Lag Coordination of Hippocampal Cell Assemblies, Neuron (2020), https://doi.org/10.1016/j.neuron.2020.05.023

The position of the animal was tracked with an OptiTrack 6-camera system (Natural Point Corp.). Calibration across cameras allowed for a three-dimensional reconstruction of the animal's head position and orientation. A rigid body was created by mounting 6 reflective markers to a small 3D-printed holder, attached to the animal's head-cap and tracked simultaneously by 6 infrared cameras (OptiTrack, Flex 3 cameras) at 120Hz.

QUANTIFICATION AND STATISTICAL ANALYSIS

Electrophysiological recordings were conducted using an Intan recording system: RHD2000 interface board with Intan 64 channel preamplifiers sampled at 20 kHz (Intan Inc).

Spike Sorting

Spike sorting was performed semi-automatically with KiloSort (Pachitariu et al., 2016) https://github.com/cortex-lab/KiloSort, using our own pipeline KilosortWrapper (a wrapper for KiloSort, https://github.com/petersenpeter/KilosortWrapper (Petersen et al., 2020), followed by a manual curation using the software Phy (https://github.com/kwikteam/phy) and our own designed plugins for phy (https://github.com/petersenpeter/phy-plugins).

Unit Classification

Well isolated units were classified into putative cell types using CellExplorer CellExplorer.org (Petersen and Buzsáki, 2020), see Figures S1L–S1O. Spiking characteristics, including the autocorrelograms, spike waveforms and putative monosynaptic connections derived from short-term cross-correlograms (English et al., 2017), were used to select and characterize well-isolated units. Three cell types were assigned: putative pyramidal cells, narrow and wide waveform interneurons.

Theta phase and phase precession

An LFP channel located in CA1 was filtered in the theta range (4-10Hz, third order butter filter, filt-filt), and translated into phase by the Hilbert transform. The phase precession slope of a place field, was determined by performing a circular-linear regression of the position versus theta phase for all spikes within the boundaries of the place field.

Oscillation Frequency of Neurons

For quantifying oscillation frequency of neurons, a 1ms-resolution spike raster was created and convoluted with an 80-point Gaussian window. The auto-correlogram was calculated and the peak between 50ms and 150ms was determined and its reciprocal value was regarded as the oscillation frequency. For place field analysis (e.g., Figures 3B, 3C, 3F, and 3H), only the spikes emitted as the animal passed through the field was included.

Place cell analysis

Spiking data were binned into 3-5 cm wide segments of the maze, generating the raw maps of spike number and occupancy probability. Place field boundaries were manually defined by the following criteria: a spatial tuned firing rate, phase precession, and peak firing rate above 10Hz. For Figure 5, place fields were automatically defined by the following criteria: at least 4 bins, where the firing rate was above 10% of the peak rate in the maze, peak firing rate > 8 Hz and spatial coherence > 0.6 (Hafting et al., 2008; Muller and Kubie, 1989).

Spatial temporal compression

To determine the spatial-temporal compression, the distance between pairs of fields (determined as the spatial distance between the spatial peak firing rate) was plotted against the temporal delay inside theta cycles (either time or phase).

The temporal offset between individual overlapping fields was determined with a 1ms bin-sized cross correlogram, convoluted with a 60 bin-wide Gaussian window. The phase offset was determined with a 0.01π bin-sized cross correlogram convoluted with a 60 bin-wide Gaussian window. The compression and oscillation period were determined by fitting the surface equation below to the density of points (Figure 5C):

$$Z = \cos\left(x\frac{2\pi}{a \cdot b} + y\frac{2\pi}{b} + 1\right) \cdot exp\left(-(x + f \cdot y)^{\frac{2}{2c^2}}\right) \cdot \exp\left(-(y - g)^{\frac{2}{2d^2}}\right) \cdot e$$

Where **a** is the compression (slope), **b** the CCG period (inverse of the oscillation frequency), **c** and **d** the widths of the two Gaussian envelopes along the x and y dimensions, **e** the amplitude, **f** the x-y shift and **g** the y-offset.

Statistical Analyses

All statistical analyses were performed with MATLAB functions or custom-made scripts. For rank order calculation, the probability of participation and firing rate correlations, the unit of analysis was single cells. Unless otherwise noted, for all tests, non-parametric two-tailed Wilcoxon rank-sum (equivalent to Mann-Whitney U-test), Wilcoxon signed-rank or Kruskal-Wallis one-way analysis of variance were used. Due to experimental design constraints, the experimenter was not blind to the manipulation performed during the experiment.

Neuron, Volume *107*

Supplemental Information

Cooling of Medial Septum Reveals Theta Phase Lag Coordination of Hippocampal Cell Assemblies

Peter Christian Petersen and György Buzsáki

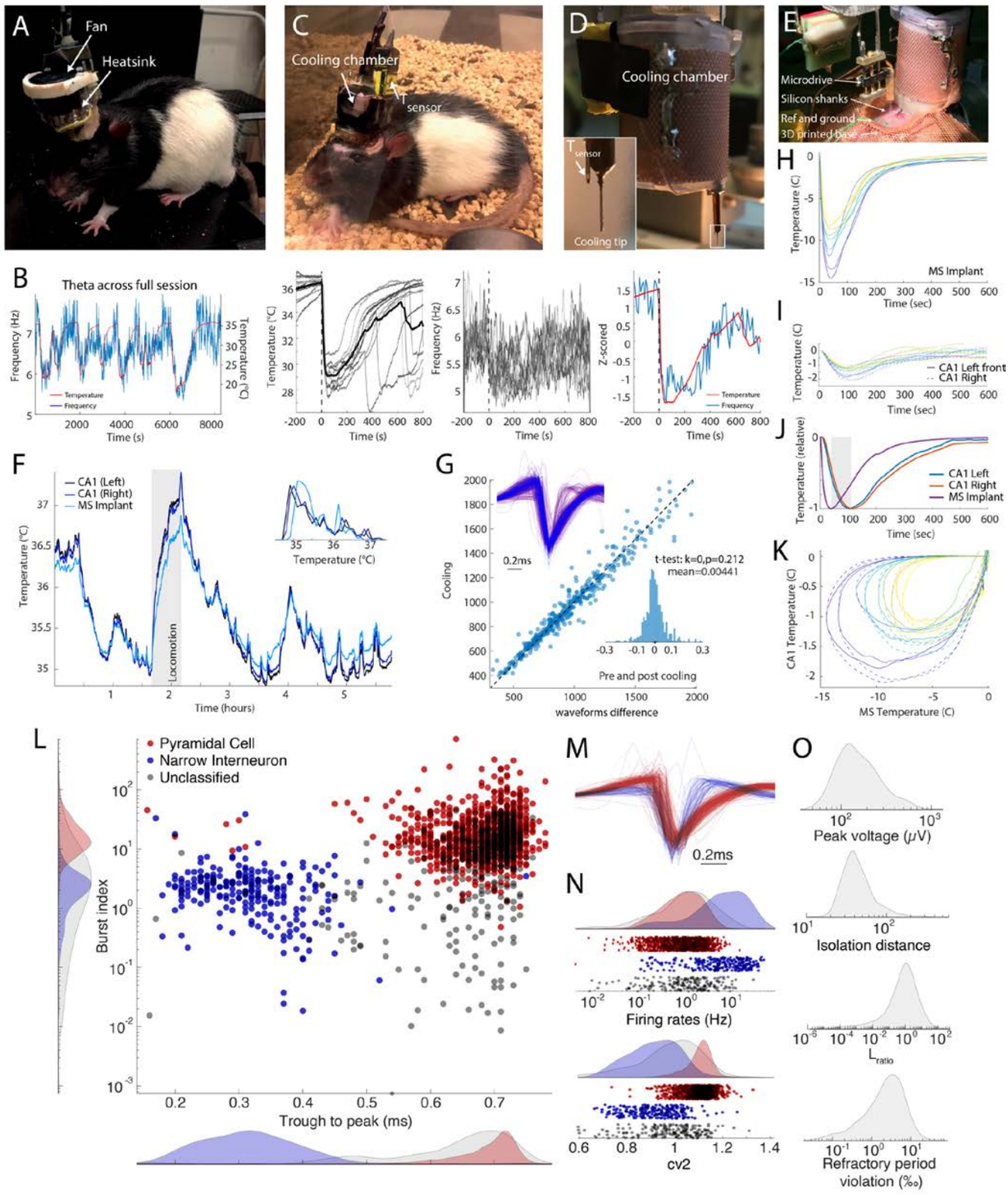

Figure S1. Methods of MS cooling. Related to Fig. 2. Two different methods for cooling the cryoprobe were tested. The first one used a Peltier device (panels A; Long and Fee, 2008). This allowed precise control of temperature over long duration and performing necessary tests of MS temperature control. However, it required both a heatsink and an electric fan for maintaining stable temperature of the Peltier element, increasing both volume and weight of the device. The second device was a small cooling reservoir (as also shown in Fig. 2A, B). This device was used in all physiological and behavioral experiments. **A**, Photograph of a Peltier device implanted in a rat. On top of the Peltier there is a small, low noise electric fan to cool the device. **B**, Relationship between MS local temperature (red) and theta frequency (blue) in the hippocampus. The MS was repeatedly cooling with dry ice. Second and third panels, successive cooling epochs are superimposed. Fourth panel, superimposed average MS temperature and frequency of hippocampal theta oscillations. Note reliable and non-accommodating relationship between MS temperature and hippocampal theta frequency across several hours. **C**, Photograph of a rat implanted with a dry iced-cooled cryoprobe. **D**, Details of the dry ice container and the cryoprobe with a temperature sensor connected to its outer tube. **E**, Photograph of the implantation with a silicon probe attached to a custom-built microdrive ready for implantation into CA1. Reference and ground screws and a 3D printed implant-base attached to the skull with meta-bond. **F**, Physiological temperature variation in the left and right hippocampus and MS. No cooling was induced in this session. Note that locomotion increases brain temperature (shaded column). Inset: Distribution of time windows spent in each

temperature unit. Note >2º C span of temperature variation. **G**, Comparison of hippocampal CA1 unit waveforms before/after (red) and during (blue) MS cooling. Inset histogram shows that MS cooling did not significantly affect unit waveforms. **H**, Magnitude and time course of MS temperature and simultaneously monitored hippocampal temperature (**I**) in successive cooling sessions in a rat. **J**, Normalized temperature curves. Note the different temporal dynamics and > 50 s delay (shaded area) between the maximum cooling effects in MS and hippocampus. **K,** Lissajous orbit plots illustrate the temporal delays of temperature effects in the MS and hippocampus. Note that the temperature scale for the hippocampus (y) is ~10 times smaller compared to the MS temperature scale (x). **L**, Scatter plot of clustered units, classified as the trough-to-peak latency of the extracellular spike (x scale) and burst index (Royer et al., 2010). The corresponding marginal histograms are shown on the left and at the bottom. Two separate clouds correspond to putative pyramidal neurons (red) and narrow spike interneurons (blue). Grey dots, unclassified neurons, not included in the statistics. **M**, Amplitude normalized, superimposed waveforms of all units. **N**, Log-firing rate distribution of the three groups (top) and distributions of the coefficient variation 2 index (CV_2) for the three groups (bottom). **O**, 'Goodness' measures of spikes. Distributions of peak voltage, isolation distance, L_{ratio} and refractory period violation.

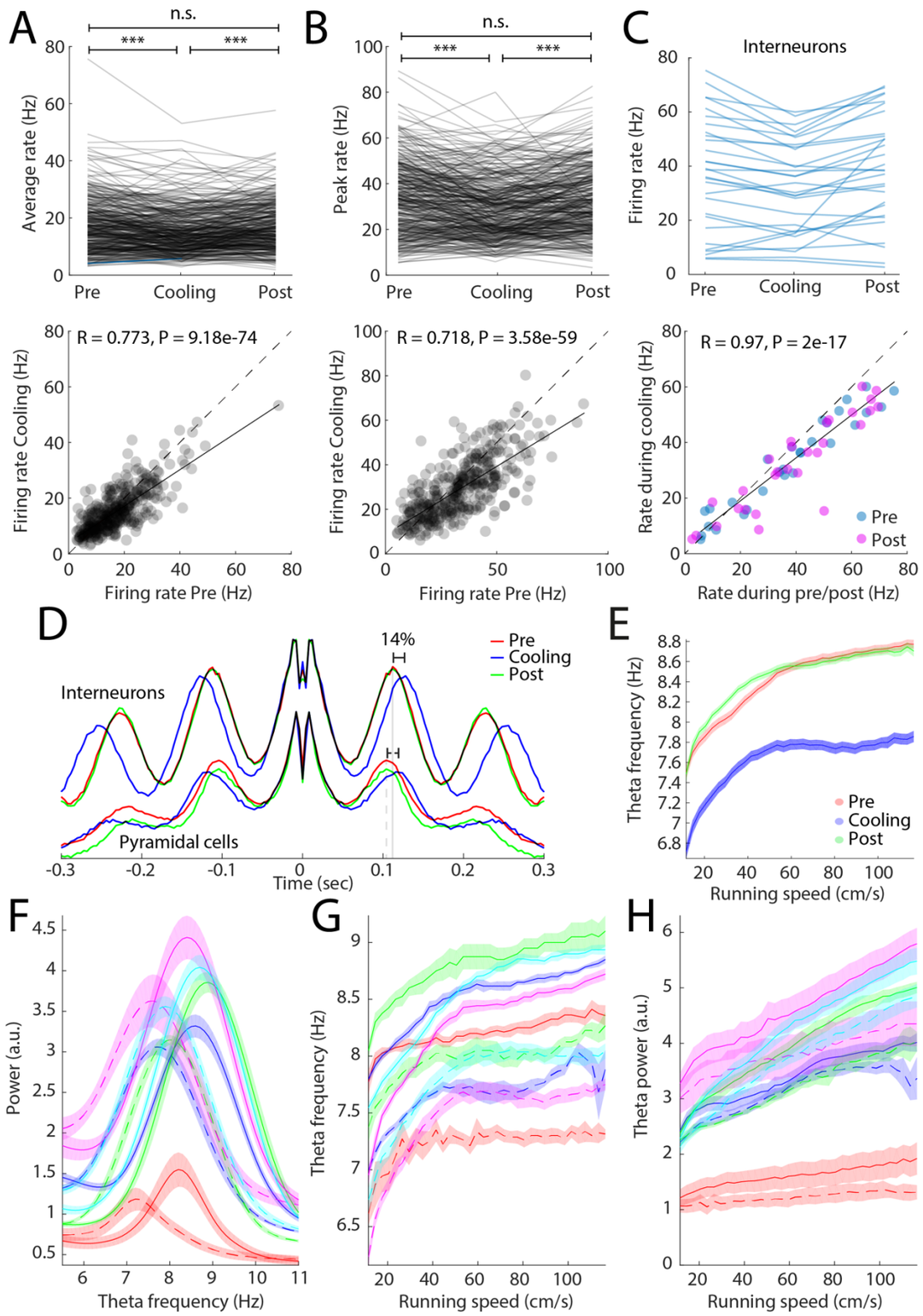

Figure S2. MS cooling affects single unit parameters. Related to Fig. 3. **A**, Firing rates of pyramidal neurons within their place fields (**A**) and their peak firing rates (**B**) (top) and illustration of the rate changes before and during MS cooling. R = 0.7, P < 10^{-58}. **C**, Same display for putative fast firing interneurons. **D**, Autocorrelograms of putative interneurons and pyramidal cells before, during and after MS cooling. Note that pyramidal neurons oscillate faster than interneurons and the theta frequency oscillation of both interneurons and pyramidal cells decreases with MS cooling by approximately 14% on average. The autocorrelograms were constructed from all spikes occurring within place fields during running for pyramical cells, and across the whole maze for interneurons. **E**, Relationship between running speed and theta frequency as the animals runs through the circular maze, unlike in Figure 3g and h, where the values were obtained from individual place fields. **F**, Power spectra for each rat before (continuous lines) and during MS cooling (dashed lines). Individual rats are color coded. **G**, Relationship between running speed and theta frequency for each rat. **H**, Relationship between running speed and theta power for each rat.

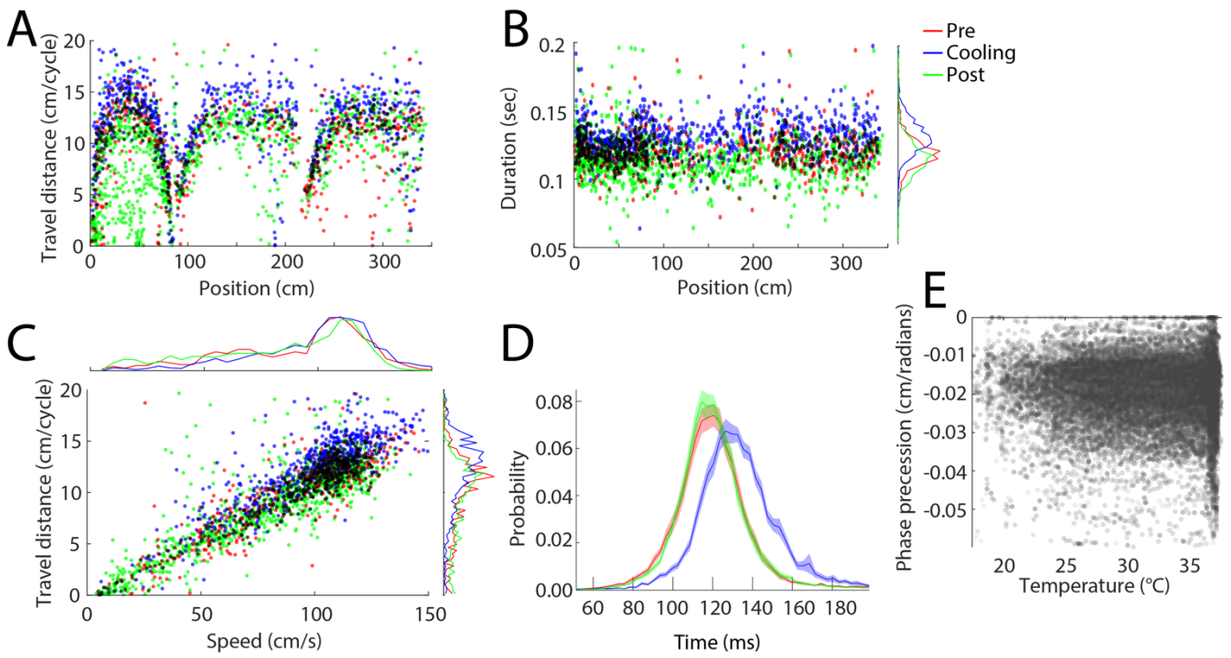

Figure S3. Speed and MS cooling affects are dissociable. Related to Figure 3. **A**, Distribution of the travel distances per theta cycle during and after MS cooling as a function of the animal's position on the track. 0-75 cm, center arm, followed by runs in the left or right arms of the maze. Note position-dependent variation of travel distances, due to speed variation on the track. **B**, Duration of the theta cycle as a function of the animal's position. Note consistently longer theta duration during MS cooling. Side histograms show longer theta cycles during MS cooling. **C**. Distance traveled per theta cycle increases with running speed. Top histogram, speed distribution before, during and after MS cooling. This session was chosen for illustration purposes because running speed of the rat remained the same during the entire session. Side histograms show that longer distances are traveled per longer theta cycles during MS cooling. **D**, Distribution of theta cycle duration for all sessions (N = 21). Note that theta cycle duration increased during MS cooling but returned after cooling to the pre-cooling control duration, even though average speed gradually decreased from the beginning to the end of sessions (see Fig. 3E, Fig. 6C). **E**, Phase precession slope as a function of MS temperature. All values from before, during and after MS cooling trials are combined. Note low (R = -0.027) but significant (P = 7.67e-19) correlation.

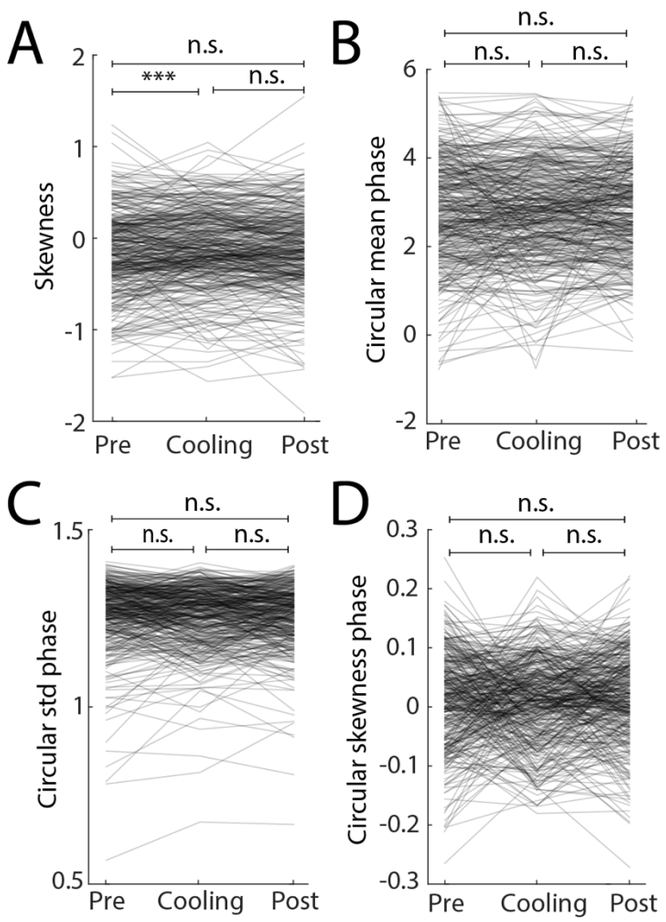

Figure S4. Properties of place fields during MS cooling. Related to Figure 4. **A, B, C, D**, Skewness, mean phase (circular mean phase), standard deviation of phase (circular standard deviation), skewness phase (circular skewness), respectively, as a function of MS cooling.

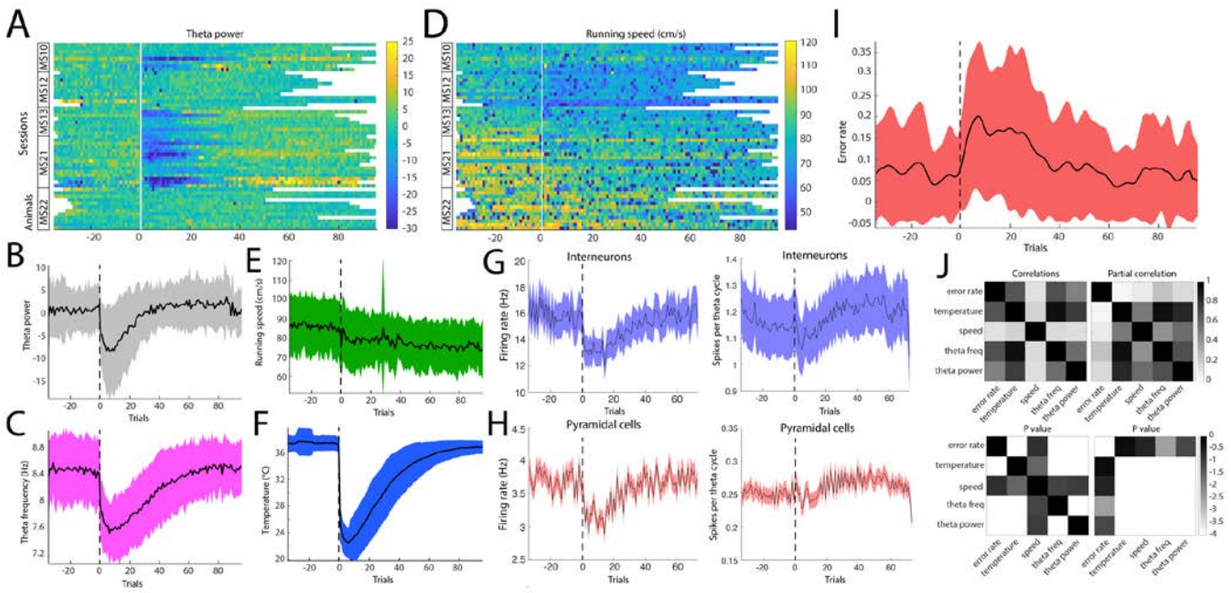

Figure S5. Time course of the effects of MS cooling on behavior and physiological parameters. Related to Fig. 6. **A**, **D**, Theta power and running speed as a function of MS cooling trials for each session. **B, E**, Group average and standard deviation related to panels **A** and **D**. Note monotonic deceleration of running speed over the entire session, likely reflecting the decreased motivation of the animal as it consumes more water cumulatively. **C, F**, **I**, Group means of theta frequency, MS temperature and choice errors, respectively. **G, H**, Trial-wise average firing rates for interneurons (**G**) and pyramidal cells (**H**) across 19 sessions with 319 interneurons and 1104 pyramidal cells. Right panels, spikes per theta cycle across the same populations. **J**, Correlation values (top) and P values (bottom) for each comparison (left

panels). Partial correlation values (top) and P values (bottom) for each comparison (right panels). Note error rates correlate best with theta frequency and have no significant relationship to running speed.

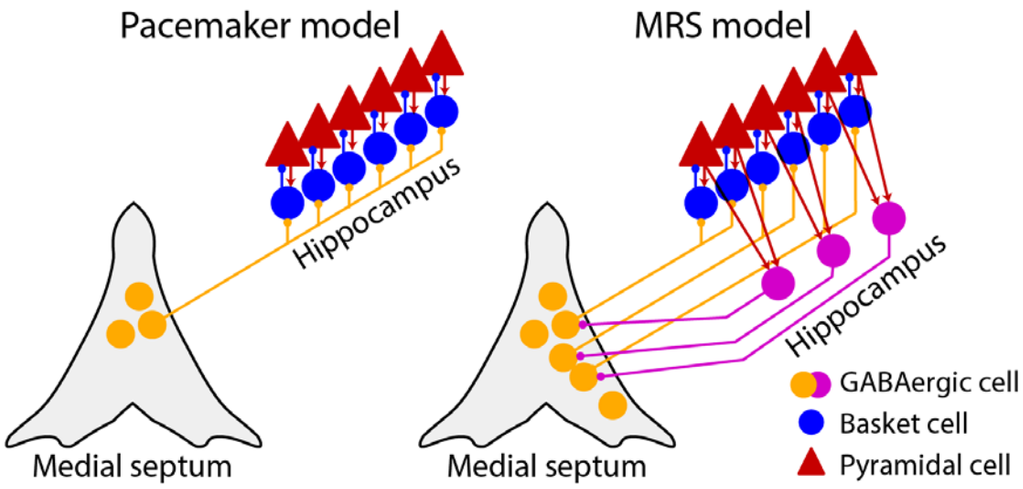

Figure S6. Related to Figure 1. Left, Traditional (pacemaker) model of MS. PV GABAergic neuronal population (PV) sends synchronous theta signal to all parts of the hippocampus by innervating interneurons (blue), which are bidirectionally connected to principal neurons (read triangles). Right, Multiple reciprocal subcircuit (MRS) model. Populations of principal neurons along the septo-temporal axis of the hippocampus project to long-range hippocampal-septum (HS) interneurons, which, in turn, loop back to MS PV neurons. In this hypothetical scheme, the multiple subcircuits in the hippocampus and MS have a topographical relationship to each other. A similar MS topography is assumed to exist in relation to the CA1–CA3–dentate gyrus axis and along dorso-ventral axis of the entorhinal cortex as well.

Animal	Recording implant	Manipulation implant	Behavioral protocol
MS6	5×50µm Single wires in CA1	Dry ice cryoprobe in MS	Wheel box
MS7	1×50µm Single wires in MS, 4×50µm Single wires in CA1	Dry ice implant in MS	Wheel box
MS8	5×50µm Single wires in MS 3×50µm Single wires in CA1	Peltier thermal device in MS	Wheel box
MS9	Cambridge Neurotech P1-64ch, 4 shanks, poly 2, CA1	Peltier thermal device in MS	Theta maze, wheel box
MS10	NeuroNexus Buzsaki 5×12	Dry ice cryoprobe in MS	Theta maze, wheel box
MS12	NeuroNexus Buzsaki 5×12 in CA1 in both hemispheres	Dry ice cryoprobe in MS	Theta maze, wheel box
MS13	Cambridge Neurotech P1-64ch, poly 2, in CA1 in both hemispheres	Dry ice cryoprobe in MS	Theta maze, wheel box
MS21	2 x NeuroNexus Buzsaki64sp, 6 shank, 10 staggered sites, implanted in CA1 bilaterally	Dry ice cryoprobe in MS	Theta maze, linear track, wheel box
MS22	2 x NeuroNexus Buzsaki64sp, 6 shank, 10 staggered sites, implanted in CA1 bilaterally	Dry ice cryoprobe in MS	Theta maze, linear track, wheel box

Table S1: Animal implants and behavioral protocols. Related to STAR Method.